ADDITIVE MANUFACTURING OF PVDF-TRFE PIEZOELECTRIC AND PYROELECTRIC SENSORS

by

Rafi Marandi

A dissertation submitted to the faculty of
The University of North Carolina at Charlotte
in partial fulfillment of the requirements
for the degree of Doctor of Philosophy in
Mechanical Engineering

Charlotte

2023

Approved by:

_____
Dr. Harish Cherukuri

_____
Dr. Stuart Smith

_____
Dr. HaiTao Zhang

_____
Dr. Maciej Noras

ABSTRACT

RAFI MARANDI. Additive manufacturing of PVDF-TrFE piezoelectric and pyroelectric sensors. (Under the direction of DR. HARISH CHERUKURI)

Additive manufacturing, specifically Fused Deposition Modeling (FDM) method, has emerged as a promising technique for rapid prototyping. Using FDM, complex geometries can be created using precise layer by layer deposition of material. Among the advantages of this method are its cost-effectiveness, rapid prototyping capabilities, and ability to customize. Due to the similar melting point of ferroelectric polymers PVDF and PVDF-TrFE to thermoplastics which are used in FDM printers, this study examined the possibility of using FDM method for additive manufacturing of piezoelectric and pyroelectric PVDF and PVDF-TrFE sensors. This method can be used in biomedical engineering, soft robotics, energy harvesting, and sensing technologies.

Although both PVDF and PVDF-TrFE can be printed by FDM, the XRD result indicated that only PVDF-TrFE crystallized in polar phase upon cooling from the melt while PVDF always crystallized in the nonpolar phase. Therefore, only PVDF-TrFE could be used for piezoelectric and pyroelectric samples. With corona poling, consistent responses from both piezo- and pyroelectric sensors were observed. Using a 30 mW laser, samples were measured for pyroelectricity. Poling at 25 kV for 10 minutes at room temperature resulted in a maximum pyroelectric response of 50 mV. The piezoelectric response of the samples was measured in both deflection mode by clamping one end and applying displacement to the free end, and also in compression mode by applying normal load to the sample placed on a flat surface. For the latter tests, d_{33} = 2.5 pC/N was found for single layer (300 μm) PVDF-TrFE. Upon impacting the free end of a PVDF-TrFE sample printed on a PVDF layer as a substrate, 130 V (peak-to-peak) of open circuit piezoelectric response was observed.

ACKNOWLEDGEMENTS

I would like to express my deepest gratitude and appreciation to several individuals who have played significant roles in the completion of my PhD dissertation.

I would like to express my sincere appreciation to my advisor, Dr. Harish Cherukuri, for his guidance and support throughout my Ph.D. dissertation. His expertise and encouragement have been invaluable in shaping my research and academic growth. I am truly fortunate to have been given this opportunity to work under his mentorship.

I would also like to extend my sincere thanks to Dr. Noras and Dr. Smith, and Dr. Zhang for their invaluable contributions as members of my dissertation committee. Your expertise, thoughtful insights, and critical evaluation have immensely strengthened the quality of my research. I am grateful for the time and effort you dedicated to reviewing my work and providing valuable suggestions for improvement.

In addition, I would like to acknowledge and express my heartfelt appreciation to my friends Faraz, Christoph, and Sami. Your support, encouragement, and willingness to lend a helping hand whenever needed have been a constant source of motivation. Your friendship and belief in my abilities have made this challenging journey more enjoyable and fulfilling.

Finally, I would like to extend my gratitude to all the individuals who have supported me in various ways, including my family, colleagues, and mentors who have provided valuable insights and assistance throughout my academic pursuit. Your encouragement, understanding, and belief in my potential have been instrumental in my success.

TABLE OF CONTENTS

LIST OF TABLES vi

LIST OF FIGURES vii

LIST OF ABBREVIATIONS ix

CHAPTER 1: INTRODUCTION 1

CHAPTER 2: LITERATURE REVIEW 4

2.1. Piezoelectricity, pyroelectricity, and ferroelectricity 4

2.2. Piezoelectric materials and their applications 6

2.3. Manufacturing methods for PVDF and PVDF-TrFE piezoelectric sensors 12

2.4. Recent research studies on FDM and inkjet printing for piezoelectric PVDF and its copolymers 19

CHAPTER 3: EXPERIMENTAL DESIGN AND METHODOLOGY 27

3.1. Printing 32

3.2. Corona Poling 39

3.3. Material Characterization 44

CHAPTER 4: RESULTS AND DISCUSSION 46

4.1. X-ray Diffractometry Results 46

4.2. Piezoelectric Response 47

4.3. Pyroelectric Response 56

CHAPTER 5: CONCLUSION AND FUTURE WORK 65

REFERENCES 70

LIST OF TABLES

TABLE 2.1: Key aspects of FDM and inkjet 3D printing methods for manufacturing of piezoelectric polymers 26

TABLE 3.1: Electrical and chemical properties of the conductive silver paint form MG chemical. 29

TABLE 3.2: Properties of PVDF-TrFE purchased from Solvay 31

TABLE 3.3: Printing settings range found to result in the best sample quality. 34

TABLE 4.1: Properties of waveforms used for the sample with substrate in one free end cantilever model 53

TABLE 4.2: Initial parameters selected for studying corona poling process. 58

LIST OF FIGURES

FIGURE 2.1: The effect of applying external electric field to the piezoelectric 5

FIGURE 2.2: PVDF chain conformation 9

FIGURE 2.3: Phase transformation in PVDF 10

FIGURE 2.4: Methods of obtaining β phase PVDF from melt, α phase 11

FIGURE 2.5: Schematic of PVDF-TrFE repeating unit 12

FIGURE 2.6: Schematic and the modified 3D printer 20

FIGURE 3.1: PVDF samples with different types of electrode 28

FIGURE 3.2: The experimental setups for direct poling in silicon oil 30

FIGURE 3.3: NEXT 1.0 filament extruder 31

FIGURE 3.4: Prusa MK2 printer 33

FIGURE 3.5: The CAD modeled samples 34

FIGURE 3.6: Schematic of 3D printing steps 35

FIGURE 3.7: PVDF-TrFE 36

FIGURE 3.8: The sample with one layer of PVDF-TrFE 36

FIGURE 3.9: Air bubble found in the purchased commercial PVDF 38

FIGURE 3.10: Print failure 39

FIGURE 3.11: Corona discharge region 40

FIGURE 3.12: Corona station with PVC tube and needle-plate setup 42

FIGURE 3.13: Improved design of corona poling station 43

FIGURE 3.14: XRD 45

FIGURE 4.1: XRD graphs 47

FIGURE 4.2: iezoelectric measurement setup 48

FIGURE 4.3: Piezoelectric respons 49

FIGURE 4.4: The experimental setup for measuring the piezoelectric response 50

FIGURE 4.5: Piezoelectric response of the sample 52

FIGURE 4.6: Stress distribution in the sample 54

FIGURE 4.7: Piezoelectric response of the double-layer sampl 55

FIGURE 4.8: Piezoelectric response of the double-layer sampl 56

FIGURE 4.9: Pyroelectric response measurement setup 57

FIGURE 4.10: he effect of corona voltage, poling time and needle-sample distance 59

FIGURE 4.11: The effect of extended poling time 61

FIGURE 4.12: Effects of poling time on pyroelectric response 62

FIGURE 4.13: Effects of sample orientation on the pyroelectric response 63

FIGURE 4.14: Common issues observed during corona poling of the samples 64

LIST OF ABBREVIATIONS

AM Additive Manufacturing

DIW Direct Ink Writing

DMF Dimethylformamide

DSC Differential Scanning Calorimetry

EPAM Electric Poling-assisted Additive Manufacturing

FDM Fused Deposition Modeling

FTIR Fourier Transform Infrared Spectroscopy

IL Ionic Liquid

IPC Integrated Corona Poling

PVDF Polyvinylidene Fluoride

SLA Stereolithography

TPPC Tetraphenylphosphonium

TrFE Trifluoroethylene

XRD X-Ray Diffractometry

CHAPTER 1: INTRODUCTION

In the years following Jacque and Pierre Curie's discovery in 1880 of piezoelectricity in crystals such as quartz and Rochelle salt, and after Langevin and his colleagues made ultrasonic submarine detectors from quartz in World War I[1], this property of specific groups of materials attracted much academic interest. Later, the advances in materials science and the development of inorganic crystals such as Barium titanate (BaTiO3) and Lead-zirconate-titanate (PZT), drastically accelerated the growth of the applications for piezoelectric materials. In 1969, Kawai found piezoelectricity in a polymer [1], Polyvinylidene Fluoride (PVDF), that resulted in the emergence of many more new applications such as flexible sensors and nonvolatile memory [2]. In 2021, just the piezoelectric devices market was estimated to be USD 28.7 billion and is projected to be USD 35.4 billion by 2026 [2]. With the discovery of piezoelectricity in new materials in recent years, researchers have also tried to develop new manufacturing methods which are more suitable for different applications. Along with the traditional methods such as the solid-state reaction process for making ceramic sensors, and the solution-casting method for polymer-based sensors, there are also novel methods proposed to either mitigate the complexity of the manufacturing process or to answer the needs for specific applications. Advances in additive manufacturing made it a very attractive option for fabricating piezoelectric sensors. Lee and Tarbutton [3] proposed the Electric Poling-assisted Additive Manufacturing (EPAM) method to directly print piezoelectric structures from PVDF polymer through Fused Deposition Modeling (FDM) printing. Their method was based on the hypothesis that non-polar

[1] https://piezo.com/pages/history-of-piezoelectricity

[2] https://www.marketsandmarkets.com/Market-Reports/piezoelectric-devices-market-256019882.html

to polar phase transformation of PVDF, resulting in piezoelectric material, would occur when applying a high electric field to the polymer while simultaneously stretching the polymer during the printing process. In this procedure, uniaxial stretching results in non-polar (α phase) to polar (β phase) phase transformation while applying a strong electric field to orient the dipoles in the polar phase. The main objective of this research is to explore the potential of using FDM method specifically for manufacturing PVDF copolymer with trifluoroethylene (PVDF-TrFE). PVDF always goes to non-polar phase when it cools down from the melt, which is happening in FDM process. On the other hand, in the same process, PVDF-TrFE behaves completely the opposite at a certain TrFE content (above 17 %mole) and always forms in polar phase, which is the desired phase for making piezoelectric sensors. As a result, this research is the first to start using PVDF-TrFE as the material for additive manufacturing samples. To achieve this objective, the following research questions were addressed:

1. Is it possible to print parts with PVDF-TrFE using FDM? This question can be approached from different aspects such as printability (adhesion, shrinkage, etc.), and the consistency of polar phase existence in the additive manufactured samples.

2. What is the most effective method for electrically pole the samples to achieve a higher piezoelectric response? Does the simultaneous printing and poling process result in strong enough electric field to form a remnant polarization in the samples?

3. What are the possible printing and poling settings which can be used to achieve repeatable results from additive manufactured sensors?

To answer these questions the following tasks were accomplished: (1) samples with simple geometries were 3D printed while printing parameters such as extrusion rate,

printing speed and direction, and overlaps between the paths, were tweaked to obtain the best possible print quality. Print quality is the most important requirement for achieving higher electric fields during poling process. (2) In order to pole the samples in a repeatable manner, a setup was designed that applied corona discharge of different intensities on the samples. In this regard, the effects of corona poling parameters, as the most effective poling method compared to direct poling, on the response of the samples were investigated via a standalone poling station. (3) material characterization analysis was performed with X-Ray diffractometry (XRD), to determine the material structure and the phase of the printed samples. In chapter two, a brief history of piezoelectricity and pyroelectricity is provided along with the introduction of the main piezoelectric materials used mainly for sensing and energy harvesting applications. With the focus on polymer-based piezoelectric materials and specifically PVDF and its copolymers, traditional and new manufacturing methods are also presented. Finally, the recent research on additive manufacturing methods for fabricating piezoelectric polymers is described. In chapter three, the testing experiments and the details regarding the sample preparation are provided. In addition to information about the printers, material properties, X-ray diffractometry, sample geometries, and printing parameters, different conductive materials as electrodes are discussed. The results of the experiments in the form of piezoelectric and pyroelectric responses of the samples are presented in chapter four. The response of single- and double-layer samples and how structural approach enhanced the piezoelectric response of the samples are explained. Also, the challenges and issues that were encountered during the tests are presented, including poling failure cases. Finally, in chapter five, the summary of this research and the key results followed by the limitations of the method, are presented. Based on these results and assumptions, future steps that might be helpful to extend the scope of the research are presented.

CHAPTER 2: LITERATURE REVIEW

The main objective of this section is to provide a review of the available literature on additive manufacturing for the fabrication of piezoelectric sensors and actuators. To achieve this goal, some fundamental concepts of piezoelectricity and manufacturing methods will be discussed in the following sections.

2.1 Piezoelectricity, pyroelectricity, and ferroelectricity

The history of piezoelectric materials dates to the 19th century, when the French physicists Jacques and Pierre Curie discovered in 1880 that certain crystals, such as quartz, possess piezoelectricity, which refers to the ability to produce an electric charge when mechanical stress is applied to them. It was this discovery that led to further research into piezoelectric materials, and in 1917 Paul Langevin developed one of the first practical applications of piezoelectricity. In World War I, Langevin used piezoelectric materials to build an underwater sonar system, which was used to detect submarines. During the 1920s and 1930s, the development of piezoelectric materials continued, as researchers discovered new ferroelectric materials such as barium titanate and lead zirconate titanate (PZT).

Piezoelectricity (from the Greek word piezein which means to press) is described as the property of materials that can generate electric charges in response to mechanical stress or strain, such as when they are pressed or stretched. Various coefficients are used to present piezoelectric response, including strain constant, d, which indicates how much polarization is induced by one unit of stress, and voltage constant, g, which measures the electrical field produced by each unit of stress. Some ceramics possess piezoelectricity due to the asymmetric arrangement of charged ions within the crystal

structure of the material, which creates a permanent electric dipole moment within its crystal structure. The potential for piezoelectricity is determined by the combination of the material's crystal structure and chemical composition [4]. When mechanical stress or deformation is applied to a piezoelectric material, it causes a shift in the positions of charged ions within the crystal lattice, which results in a change in the electric polarization of the material. It is through this change in polarization that a net electric charge is generated in the material, which can be utilized to produce an electrical signal based on the change in polarization. The application of an electric field can, on the other hand, result in a deformation or mechanical movement in the material, giving rise to the property of inverse piezoelectricity. Eleven of the 32 crystal classes are centrosymmetric and therefore cannot have polar properties. With the only exception of point group 432, there are 20 piezoelectric classes remaining in which the center of symmetry does not exist. Only 10 of these 20 classes have unique polar axes that result in spontaneous polarization, and these are pyroelectric materials.

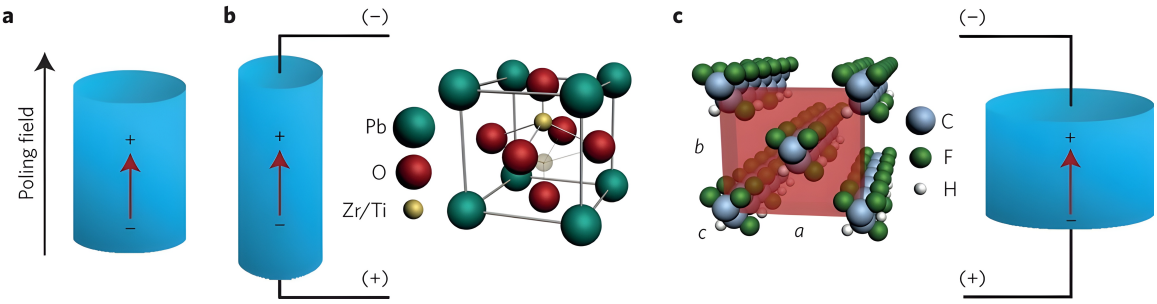

Figure 2.1: The effect of applying an external electric field to the piezoelectric materials: equilibrium state (a), ceramics such as PZT (b), and polymers such as Polyvinylidene fluoride (PVDF) (c). Image taken from [5]

As the name suggests, pyroelectricity is a property of certain materials that is caused by temperature changes, and due to temperature-induced changes in the crystal structure of a material following a change in temperature, the polarization of the material can also alter, resulting in a net electric charge due to the change in

polarization. Also, ferroelectric crystals, which are a class of materials that exhibit spontaneous electric polarization that is reversible once an external electric field is applied, are all pyroelectric crystals, but not all pyroelectric crystals are ferroelectric crystals. As a result of a change in temperature, ΔT , there is a change in polarization, ΔP . The pyroelectric coefficient, p, relates these two parameters via $p = \Delta P/\Delta T$. There are two ways in which polarization changes because of a change in temperature can be measured. The primary pyroelectric coefficient is the pyroelectric coefficient that is measured when the crystal dimensions are held constant, that is, at constant strain, when the pyroelectric coefficient is measured. A secondary pyroelectricity contribution can be observed when the crystal dimensions are allowed to change, which is the result of the crystal dimensions changing [6]. For a polymer to exhibit pyroelectricity, it needs to have molecular dipoles that are arranged in a specific manner. Additionally, the alignment of these dipoles must remain stable over time and under varying temperatures. Consequently, any polar polymer has the potential to demonstrate pyroelectric properties [7].

2.2 Piezoelectric materials and their applications

Since the discovery of piezoelectricity in quartz and Rochelle salt by Jacque and Pierre Curie in 1880, this property has been the focus of academic research and industrial applications. There is a considerable influence on the performance of piezoelectric systems based on the type of material that is selected. With material science advances and inorganic crystals such as Barium titanate (BaTiO3) and Lead-zirconate-titanate (PZT) being developed, piezoelectric material applications grow rapidly. After Kawai's discovery of piezoelectricity in Polyvinylidene fluoride (PVDF) in 1969 [1], many novel applications such as flexible sensors and nonvolatile memory were developed. Nonorganic piezoelectric ceramics (e.g., PZT) are typically fabricated using a solid-state reaction process, which involves mixing the raw materials, compacting them into the desired shape, and sintering them at high temperatures

to form a dense ceramic material. The final properties of the ceramic material are determined by the composition, microstructure, and processing conditions [4]. The unique properties of ceramic piezoelectric materials, including high piezoelectric coefficients ($\sim 100 - 500$ pC/N), mechanical hardness, and chemical stability, make them suitable for use in a variety of fields. They are used in a wide range of devices, such as ultrasonic transducers [8], pressure sensors [9], and vibration sensors [10]. Ceramic piezoelectric materials also have potential applications in energy harvesting [11], where they can convert ambient mechanical vibrations or thermal energy into electrical energy. Additionally, these materials have potential applications in bioengineering, such as ultrasound imaging [12]. Ceramic piezoelectric materials are also used in precision positioning and control systems, where their high resolution and fast response time make them suitable for micro- and nano-scale applications such as acoustic and vibration damping, where they can reduce the level of noise and vibration in mechanical systems [13].

Despite their many advantages, ceramic piezoelectric materials also have several limitations that limit their potential applications. The brittle nature of these materials makes them prone to cracking and fracture under mechanical stress. Because of this, they cannot be used in applications that are subject to high mechanical stress, such as structural health monitoring. In addition, their relatively high density makes them unsuitable for lightweight applications. Also, some nonorganic piezoelectric ceramics contain lead, and due to their toxicity and its risk to human health and the environment, more restrictions in recent years have been applied to their usage. To overcome this issue, new lead-free ceramics such as compositions based on potassium sodium niobate family (K, Na)NbO3 or KNN, have been developed [14].

Following Kawai's discovery of piezoelectricity in PVDF, increasing attention has been paid to ferroelectric polymers (EAPs). This includes piezoelectric polymers such as Nylon-11 and poly(L- lactic acid) (PLLA) [15]. There are several advantages

to these materials over traditional nonorganic piezoelectric ceramics, including their flexibility, low density, biocompatibility, ease of processing, and lead-free. Due to their unique properties, polymer-based piezoelectric materials can be used in wearable devices, biomedical engineering, energy harvesting, structural health monitoring, and human-machine interfaces [16, 17, 18, 19, 20].

PVDF is a semi-crystalline thermoplastic polymer that is composed of carbon, hydrogen, and fluorine atoms. The polymerization of the monomer vinylidene difluoride forms the polymer chains that have the molecular formula of $(CH_2 - CF_2)_n$ where n represents the number of repeating units. There are two hydrogen atoms and two fluorine atoms bonded to each carbon atom in the molecular structure. Different processing conditions and cooling rates result in different phases and crystal structures in PVDF [21]. PVDF can crystallize into at least three different configurations: TGTG[1] in the α and δ phases, a flat zigzag arrangement with all trans (TTT) in the β phase, and T_3GT_3G in the γ and ϵ phases. PVDF most commonly forms in two crystallized phases: α-phase and β-phase. The α-phase is the most stable and thermodynamically favored (lowest energy) phase of PVDF when cooled down from the melt under room temperature and pressure [22], while β phase is formed under certain processing conditions such as high-temperature crystallization [23], and annealing [24]. In the α-phase, the PVDF molecules are arranged in a crystalline structure that is symmetric along the chain axis, with the fluorine atoms and the hydrogen atoms distributed evenly on opposite sides of the chain. This symmetry results in a molecular structure that does not have a net dipole moment, and therefore making it non polar [25]. In the β phase, the PVDF molecules are arranged in a planar zigzag structure, with

[1]Trans (T) and gauche (G) conformations are specific arrangements of substituent groups or atoms around a single bond in a molecule, commonly found in organic chemistry. The trans conformation refers to a configuration where the substituent groups or atoms are positioned on opposite sides of the bond. This arrangement results in a linear or extended shape of the molecule. On the other hand, the gauche conformation describes a configuration where the substituent groups or atoms are located on the same side of the bond. This arrangement introduces a bend or a kink in the molecule due to steric hindrance or repulsion between the groups.

fluorine atoms and hydrogen atoms aligned alternately on opposite sides of the chain. This arrangement results in a net dipole moment, making the β phase of PVDF polar. This phase can be formed by processing PVDF under specific conditions, such as mechanical stretching or manufacturing methods such as electrospinning [21].

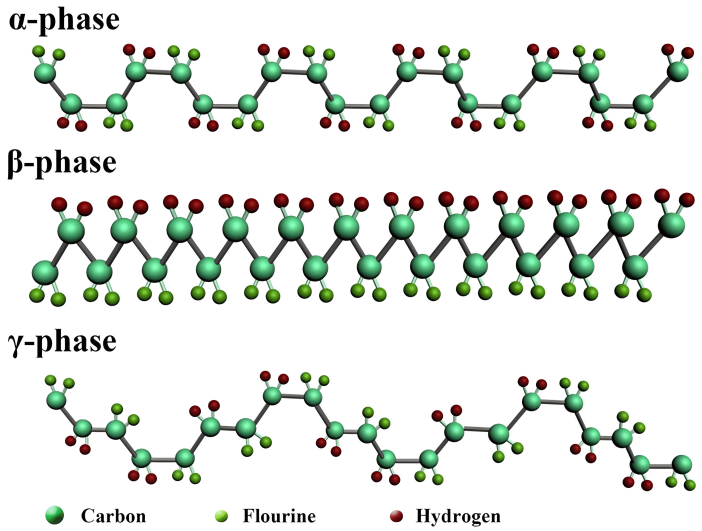

Figure 2.2: : PVDF chain conformation for α-, β- and γ-phase. Image taken from [26]

Based on the processing conditions and cooling rate, PVDF can also exhibit other structural phases than α and β-hase, including:

γ-phase: The γ phase is a non-crystalline or amorphous phase that is formed when PVDF is processed at high temperatures or under high pressure. The γ phase does not exhibit any long-range order, and its properties depend on the processing conditions [27].

δ-phase: The δ phase is a polar phase that is formed when PVDF is subjected to a strong electric field or high-pressure treatment. δ-phase has the same chain conformation as α-phase, however, in α phase, all contributions nullify each other, while in the δ phase, although the components within the plane cancel each other out, the components perpendicular to the plane result in a measurable dipole moment [28]. The δ phase exhibits a unique crystal structure that is characterized by alternating

planes of trans and gauche conformation [21].

ϵ-phase: The ϵ-phase is a non polar phase that is formed when PVDF is stretched or oriented at high temperatures. The ϵ-phase exhibits a unique crystal structure that is characterized by a helical arrangement of the polymer chains [29].

The crystalline structure of PVDF can change and therefore it can be transformed from one phase to another under certain conditions such as temperature, pressure, or mechanical stress. Phase transformations in PVDF can also be induced by various methods such as mechanical stretching, electrical poling, annealing, or solvent treatment. The process involves breaking and reforming inter- and intramolecular hydrogen bonds, leading to a change in the molecular conformation [30, 31, 32].

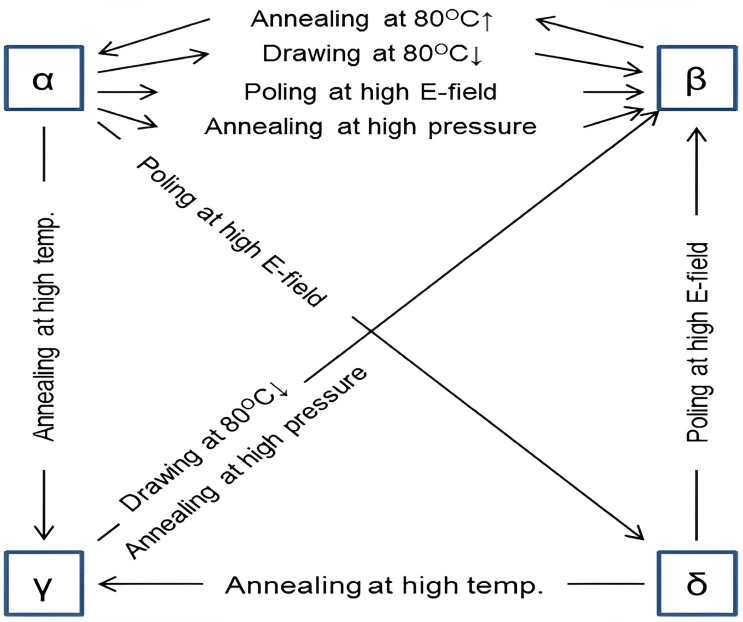

Figure 2.3: Phase transformation in PVDF. Image taken from [33]

The β-phase has the highest dipolar moment per unit cell (8×10^{-30} C.m) when compared to the other phases which makes it the most desired phase for applications involving piezoelectricity [21]. There are several processing conditions that influence the formation of the beta-phase in PVDF, including cooling rates and stretching. Cooling rate is one of the critical factors that influence the formation of the β-phase.

Slow cooling rates below a certain threshold do not result in the formation of the β-phase, whereas rapid cooling rates above a certain threshold can result in the formation of the β-phase [34]. Stretching the α-phase of PVDF above a certain threshold can cause the polymer chains to align in a planar zigzag arrangement, resulting in the formation of the β-phase[31]. The stretching can be accomplished using various techniques, such as uniaxial or biaxial stretching, and the degree of stretching and the stretching rate can influence the properties of the resulting β-phase [31, 35, 36].

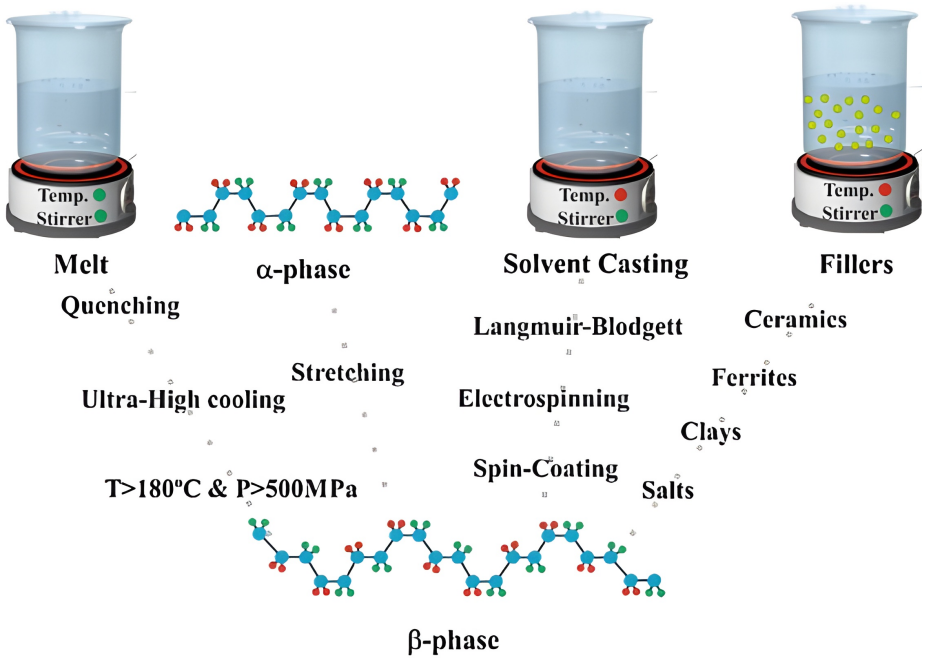

Figure 2.4: :Methods of obtaining β phase PVDF from melt, α phase, and preparation methods. Image from [21]

High external electric fields applied to PVDF, can also initiate phase transition from α phase to β-phase. This phenomenon is known as the electric-field-induced phase transition (EFIT) and has been extensively studied for PVDF homopolymer and its copolymers [30, 37, 38, 39]. EFIT can produce a highly oriented β-phase PVDF with unique piezoelectric and mechanical properties. It is possible to control orientation and phase formation by varying the strength, frequency, and duration of the electric field [40]. Nevertheless, applying very high electric fields can also lead to

material degradation and electrical breakdown [41].

The addition of trifluoroethylene (TrFE) units to PVDF can promote the formation of the β-phase during the polymer processing [42]. TrFE is a fluorinated monomer that can copolymerize with PVDF to form PVDF-TrFE copolymers. Incorporating TrFE units into PVDF polymer chains alters the conformation of the chains and reduces the energy barrier necessary to form the β-phase. Therefore, all trans conformation characterizing β-phase is more favorable in PVDF-TrFE copolymers than in PVDF homopolymers [43]. Moreover, the amount of TrFE units in the copolymer can be adjusted to control the degree of β phase formation and the resulting properties [44]. Studies have shown that a minimum TrFE content of 15-20% is required to promote the formation of the β-phase in PVDF-TrFE copolymers [42]. With TrFE contents below this threshold usually exhibit α-phase crystallization or the formation of the γ-phase [15]. PVDF-TrFE exhibit enhanced piezoelectric properties, making it suitable for piezoelectric sensors and actuators [45].

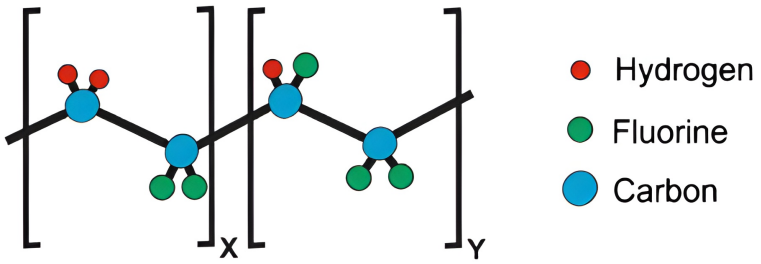

Figure 2.5: Schematic of PVDF-TrFE repeating unit. Image from [21]

2.3 Manufacturing methods for PVDF and PVDF-TrFE piezoelectric sensors

Piezoelectric PVDF sensors have gained significant attention in various industries due to their unique properties such as lightweight, flexibility, and high sensitivity. These sensors are capable of converting mechanical stress or vibrations into electrical signals, making them ideal for applications in pressure sensing, acoustic sensing, vibration monitoring, and energy harvesting. The performance of these sensors depends on

the crystalline phase of the polyvinylidene fluoride (PVDF) material, specifically the polar β-phase. As a result, numerous manufacturing and preparation methods have been developed to fabricate piezoelectric PVDF sensors, ensuring the formation of the desired β-phase to optimize the sensor's performance. These methods encompass a variety of techniques, including solution casting, electrospinning, melt processing, and layer-by-layer assembly, each offering its advantages in terms of scalability, control over film thickness, and the ability to create complex structures or integrate other materials. In this section, a brief description of the conventional methods is discussed followed by the recent advances in additive manufacturing for piezoelectric sensors.

Solution casting: Solution casting is a common method used to manufacture piezoelectric polymer sensors. In this method, the polymer is first dissolved in a suitable solvent, such as dimethylformamide (DMF) or N,N-dimethylacetamide (DMAc), to form a viscous solution [46]. The solution is then cast onto a substrate, such as glass or silicon, and allowed to dry. The drying process can be performed by evaporation of the solvent at room temperature or by heating the substrate to remove the solvent more quickly. One of the advantages of solution casting is that it is a relatively simple and inexpensive method. The polymer solution can be easily prepared, and the casting process can be performed using basic equipment. Moreover, solution casting can produce thin films with a wide range of thicknesses, making it suitable for a variety of applications. However, there are also some limitations to the solution casting method. One of the main challenges is achieving uniform thickness and quality of the film. Variations in the casting process, such as the speed of casting, temperature, and humidity, can result in non-uniform thickness and defects in the film. In addition, the choice of solvent can also affect the properties of the resulting film, and some solvents may be hazardous or difficult to handle. Despite these limitations, solution casting remains a popular method for manufacturing piezoelectric polymer sensors due to its simplicity and low cost. Researchers continue to investigate ways to improve the uni-

formity and quality of the films produced by solution casting, such as using additives or controlling the casting conditions more precisely [47].

Spin coating: Spin coating is another method used to manufacture piezoelectric polymer sensors. In this method, a solution of the polymer is deposited onto a substrate, and the substrate is spun at high speeds to spread the solution into a thin and uniform layer. The film is then subjected to mechanical or thermal treatment to induce the β-phase and enhance the piezoelectric properties [48]. The spinning speed and duration can be controlled to adjust the thickness of the film. One of the advantages of spin coating is that it can produce thin films with a high degree of uniformity and control over the thickness. This method is suitable for producing films with thicknesses ranging from a few nanometers to several micrometers [49]. Moreover, spin coating can be performed using relatively simple equipment and is a scalable method for mass production. However, spin coating also has some limitations. For example, it may not be suitable for producing large-area films, and the thickness of the film can be affected by variations in the spinning speed and duration. In addition, the method may not be suitable for producing complex patterns or shapes. Despite these limitations, spin coating remains a popular method for manufacturing piezoelectric polymer sensors, especially for applications that require thin and uniform films, such as energy harvesting and biomedical sensing.

Electrospinning: Electrospinning is a unique method used to manufacture piezoelectric polymer sensors. In this method, by applying a high voltage to a polymer solution, the induced electric field overcomes the surface tension of the droplets, causing the jet of polymer solution to elongate into a cone-shaped jet, called Taylor cone. In the grounded collector, thin polymer fibers are randomly displaced as the solution evaporates [50]. The diameter of the fibers can be controlled by adjusting the voltage, flow rate, and distance between the electrode and substrate [51]. One of the advantages of electrospinning is that it can produce fibers with a high degree of

alignment and uniformity. The method can also produce fibers with a diameter ranging from a few nanometers to several micrometers, making it suitable for a variety of applications. Moreover, the non-woven mat produced by electrospinning can have a high surface area-to-volume ratio, which can enhance the sensing performance of the resulting sensors. However, electrospinning also has some limitations. Choosing the right solution parameters as well as electrospinning values, can affect the β-phase content and prevent issues such as jet disruption due to syringe clogging [50]. The process can be challenging to control, and the diameter and alignment of the fibers can be affected by variations in the processing conditions. Moreover, electrospinning may not be suitable for producing large-area films or complex patterns.

Printing: Printing techniques such as Inkjet printing is a method used to manufacture piezoelectric polymer sensors that involves the deposition of ink onto a substrate in a precise pattern using an inkjet printer. The deposited polymer can then be subjected to mechanical or thermal treatment to induce the β-phase and enhance the piezoelectric properties [52]. The ink used for printing contains a polymer solution with piezoelectric properties, which can be deposited in a controlled and repeatable manner to produce the desired pattern or shape. One of the advantages of inkjet printing is that it can produce complex patterns and shapes with a high degree of precision and reproducibility. This method is also scalable and can be easily adapted for mass production. Moreover, inkjet printing can be used to deposit multiple materials in a single step, allowing for the production of multilayered or composite sensors [53]. However, inkjet printing also has some limitations. The viscosity and surface tension of the ink can affect the print quality, and some inks may clog the printer nozzles. Moreover, inkjet printing may not be suitable for producing thick films or large-area sensors.

Additive Manufacturing (AM): Additive manufacturing, also known as 3D printing, has emerged as a promising approach for fabricating piezoelectric polymer

devices [54]. This technique enables the creation of complex structures, rapid prototyping, and customization of device designs. Since this method is the focus of this research, a brief general explanation of additive manufacturing is provided below. For an object to be 3D printed using any additive manufacturing technique, the 3D model must be converted into a format that the 3D printer can understand. This process involves two main steps: slicing and generating G-code. These steps can be performed automatically by the printer or manually by the user, depending on the method and other factors like the user interface or complexity of the printer. Slicing is the first step in preparing a 3D model for printing. The first step in preparing a 3D model for printing is slicing. This process involves dividing a 3D model into thin horizontal layers. A layer represents a cross-sectional area of an object that will be constructed sequentially, one on top of another, by the printer. Slicing is performed using specialized software, known as slicers, which take the 3D model (usually in formats such as STL, OBJ, or 3MF) and generate a set of instructions for the printer to follow. As part of the slicing process, printing parameters are set based on factors such as the material, desired resolution, print speed, and others. There are several parameters to consider, including layer height, which determines the resolution along the Z-axis, infill density, which affects the object's strength and weight, and support structures, which are necessary for overhanging features that cannot be printed without temporary support.

As soon as the 3D model is sliced, the slicer software generates a set of instructions called G-code which is specific to the machine. G-code is a widely used numerical control programming language for computer-controlled machines, including 3D printers. Each line of G-code represents an action or a series of actions that must be taken by the 3D printer. This includes the movement of the extruder, setting the temperature, and other printer-specific operations. For instance, G-code commands may specify extruder coordinates, the temperature at which it should heat, the speed at which it

should travel, or when to retract the filament to prevent stringing. Once the G-code file has been created, the file can then be loaded into the 3D printer via USB, SD card, or network connection. During the printing process, the printer's firmware reads the G-code generated by the software and executes each line of commands line by line, layer by layer, until the printed object reaches its final state. There are several additive manufacturing methods suitable for making piezoelectric polymer devices [55].

1. Fused Deposition Modeling (FDM): FDM is a widely used 3D printing technique that involves extruding a thermoplastic filament through a heated nozzle and depositing it layer-by-layer onto a build platform. For piezoelectric devices, the PVDF or PVDF-based composite filament can be used. Post-processing, such as poling, is required to align the dipoles and induce the piezoelectric β phase. FDM allows for the fabrication of devices with intricate geometries and varying thicknesses, although the resolution may be limited by the nozzle size [3].

2. Stereolithography (SLA) or Digital Light Processing (DLP): Both SLA and DLP are resin-based 3D printing techniques that utilize a light source (laser or projector) to selectively cure a photosensitive polymer resin. To fabricate piezoelectric devices, the resin can be formulated with PVDF or its copolymers and piezoelectric nanoparticles. The cured parts require post-processing, including washing, curing, and poling, to induce the piezoelectric β phase [56]. SLA and DLP offer higher resolution and surface quality compared to FDM, but the availability of piezoelectric resins and the requirement for additional post-processing steps may pose challenges.

3. Direct Ink Writing (DIW) or Extrusion-based 3D printing: In this method, a paste or gel-like ink containing PVDF or PVDF-based composites is extruded through a nozzle and deposited onto a substrate in a layer-by-layer fashion

[57]. The ink formulation must ensure proper rheological properties to maintain the shape and structure during printing [58]. Post-processing steps, such as drying, sintering, and poling, may be required to induce the piezoelectric β-phase. DIW enables the fabrication of complex, multi-material structures and offers scalability for larger devices, but the resolution may be limited by the nozzle size and ink properties.

Additive manufacturing methods have the potential to revolutionize the fabrication of piezoelectric polymer devices, enabling rapid prototyping, customization, and complex geometries that are difficult to achieve with traditional manufacturing techniques. However, challenges such as material availability, resolution limitations, and the need for post-processing steps to induce the piezoelectric properties must be addressed to fully exploit the advantages of these techniques. Next, the most recent research works implementing FDM and inkjet printing methods, as the main additive manufacturing methods for PVDF and its copolymers, and as the focus of this research, will be discussed.

2.4 Recent research studies on FDM and inkjet printing for piezoelectric PVDF and its copolymers

FDM and ink printing (based on solvent evaporation) are two distinct additive manufacturing techniques used for manufacturing PVDF-based piezoelectric sensors. It is to this end that some of the pioneer and recent studies that utilized these AM techniques are presented in this section. The key aspects of these studies (e.g. manufacturing method, poling condition, etc.) are provided in Table 2.1 at the end of this section.

Lee and Tarbutton [3] developed Electric Poling-assisted Additive Manufacturing (EPAM) to print piezoelectric structures directly from PVDF polymer using Fused Deposition Modeling (FDM). By applying a strong electric field to polyvinylidene fluoride (PVDF) rods, they succeeded in printing piezoelectric devices directly and continuously. Continuously fabricating piezoelectric devices is possible through EPAM, which combines AM with electric poling. By using this method, PVDF polymer dipoles stay aligned and uniform over a large area during design, production, and fabrication. Under high temperatures, the leading nozzle applies mechanical stress in situ to the molten PVDF polymer while applying high electric fields to pole it electrically. A piezoelectric structure can be directly printed using the EPAM system while a high electric field is applied between the nozzle tip and the printing bed in AM machines.

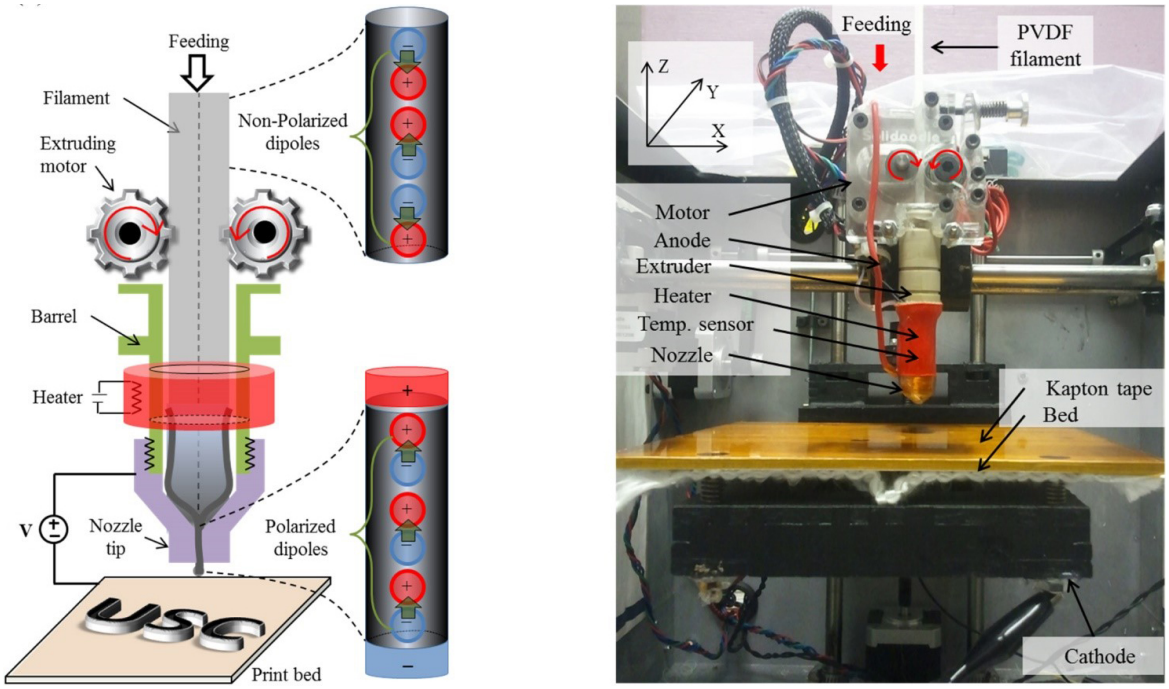

(a) (b)

Figure 2.6: Schematic (a) and the modified 3D printer (b) of electric poling-assisted additive manufacturing (EPAM). Image taken from [3]

To study the effect of electric field conditions on the piezoelectric characteristics of PVDF polymer, 100 mm long devices were printed under four different electric field conditions: no electric field, 1.0 MV/m, 2.0 MV/m, and 3.0 MV/m. It was reported that cyclic bending by hand, the samples which are poled under 1.0 MV/m and 2.0 MV/m, the output current was ± 0.25 nA and ± 0.37 nA, respectively. As a result of 3.0 MV/m, an electrical breakdown occurred, and poling could not be sustained. Their initial results led them to fabricate a larger sample on a flexible substrate that generated ± 1.5 nA. Samples fabricated under three different electric poling conditions also showed improved crystalline phases with higher applied electric fields. A Fourier Transform Infrared Spectroscopy (FTIR) analysis indicates that PVDF polymeric filament before extrusion shows nearly identical results without an electric field applied

Porter et al. [59] investigated the effects of FDM printing parameters on the proper-

ties of 3D-printed PVDF films. Through tensile testing and digital image correlation (DIC) analysis, they examined the influence of in-fill angle on Young's Modulus, Poisson's ratio, and yield strength. FTIR was also used to analyze β-phase content in relation to processing parameters. It was found that a higher β-phase content was associated with a lower extrusion temperature, higher extrusion rate, and higher hot-end voltage while post-printing corona poling induced a small but consistent piezoelectric response in mainly β-phase films. According to their study, Young's modulus for 3D printed PVDF samples was between 457 and 486 MPa, with an average Poisson's ratio of 0.305. Several factors influenced beta-phase content, including temperature, bed material, and horizontal speed. The piezoelectric coefficient d_{31} in high β-phase content PVDF films generated by electrical poling at 80 °C under an oil bath field of 8.33 MV/m was repeatable, despite its small value. Using a modified FDM method with integrated corona poling (IPC), Kim et al. [60] fabricated PVDF piezoelectric films for sensor applications. Following the printing of layers, the nozzle at 250 °C and connected to high voltage follows the same path as the printing path used for the printed sample without extruding material. For the electrical poling step, the nozzle ionized the air close to the nozzle and placed the charges on the sample at a temperature of 60 °C. To characterize the piezoelectric properties of the IPC PVDF films, FTIR analysis, and fatigue load frames were used. FTIR analysis shows that stronger electric voltage resulted in higher β-phase content in the samples and therefore produced greater current output and piezoelectric coefficient d_{31} of 4.8×10^{-2} pC/N for samples under 12 kV. As a result of the IPC process developed in this research, the piezoelectric output current can reach a value of 0.001 nA during the IPC process while applying 12 kV of electric voltage. In addition, Kim et al. It was found that the ultimate strength of the IPC PVDF film after the IPC process under 12 kV increased from 17-19.8 MPa. In contrast, the strain decreased from 45.4% to 38.6%. In addition, it was found that increasing the heating bed temperature reduces

the piezoelectricity of the PVDF film. From the tensile testing results, it was discovered that the ultimate strength of the IPC PVDF film is enhanced after the IPC process due to molecular structure changes. Based on the results, the IPC process can produce piezoelectric PVDF film.

Yuan et al. [61] used the ink-deposition method to fabricate approximately 10 μm thick PVDF-TrFE layers using a self-made printer. The process involved multiple steps: First, a silver electrode layer was 3D printed onto a flexible polyimide (PI) film, which was solidified at 80°C for 20 minutes. Then, a solution of PVDF-TrFE (with a 70/30% mole ratio) in Dimethyl sulfoxide and acetone was printed using another nozzle. The final step involved corona poling, where the platform was moved under a corona needle (15 kV) and a mesh (5 kV) for 3 minutes. These steps were repeated six times to achieve six layers with a PVDF-TrFE film thickness of 60 μm. This film was wrapped around a 3D printed "rugby ball" structure to increase the stress introduced to the piezoactive film.

The rugby ball-structured multilayer PVDF-TrFE composite film exhibited a high peak output voltage of 88.6 V_{pp} under a pressure of 0.046 MPa in the low-frequency range, which is almost two times that of a flat single-layer PVDF-TrFE structure. The observed piezoelectricity was as high as 130 pC/N from the sample, which is six times higher than that from a single PVDF-TrFE film (d_{33} = 22 pC/N). The piezoelectric coefficient d_{33} of alpha-PVDF is only 3 pC/N. It should be noted that the peak output power density as an energy harvester unit was as high as 16.4 mW/cm^2 in short circuit condition and 5.81 mW/cm^2 under the load of 568 kΩ.

Tarbutton et al. [62] also studied the phase transformation of PVDF during the additive manufacturing process (EPAM). Using Fourier Transform Infrared Spectroscopy (FTIR) and Differential Scanning Calorimetry (DSC), the authors investigated the phase changes of PVDF filament before printing, printed samples under no external electric field, and printed samples under 30 MV/m.According to FTIR

and DSC results, EPAM method changes the crystalline phases combination (mainly α, β, and δ).The result shows the 35% crystalline of PVDF in which approximately 35% is in β phase and no γ phase in all the samples. Also due to similarity of α and δ phases, they hypothesized that it is possible that some of the α phase transforms into δ phase because of polymer chain reorientation, during printing process under high electric field. Considering the results of both methods, the authors concluded that EPAM can induce the change of non-polar α phase to either amorphous or other phases. Furthermore, in this study, two shock sensors (1-layer and 2-layer) were manufactured using the EPAM method (under 30 MV/m) and with silver epoxy was applied to the samples as the electrode to measure the generated charge due to impact. The measured d_{33} was 0.66 pC/N and 0.23 pC/N for for 1- and 2-layer samples, respectively. By acknowledging the fact that PVDF tends to form in the α-phase when it solidifies from the melt, Liu et al. [63] proposed a method to obtain β-phase for 3D printed samples using FDM. In this method, PVDF pellets were mixed with an ionic liquid (IL) agent (1-ethyl-3-methylimidazolium tetrafluoroborate) through stirring in N,N-dimethylformamide (DMF, 99.5%) solvent. The interaction between positive imidazole ions and CF_2 dipoles facilitates the formation of an all-trans conformation of the β-phase. The prepared solutions with different quantities of IL (0-20 wt%) were dried by placing them in an oven overnight and then converted into a filament using an extrusion device at 200 °C. Due to the high conductivity of the IL, which results in higher dielectric loss of the material and therefore higher energy loss, the 3D printed samples were immersed in a water bath at 70 °C for 2 hours. The β-phase content in the final samples was measured via FTIR and the method presented by [31]. Based on the reported results, adding 15 wt% of IL resulted in increasing the β-phase content to 93% compared to 13.5% of pure PVDF. The piezoelectric response of the samples was evaluated by applying normal stress to them and measuring the generated charge with an oscilloscope. The maximum open circuit

voltage of 3 V and short circuit current of 55.5 nA were measured for the sample with a thickness of 0.8 mm and 20 wt% of IL. As a structural approach, a sample with hemispherical protrusion features on the top surface was also fabricated, which showed 4.2 V and 71 nA under the same stress. In a similar study, Pei et al. [64] used tetraphenylphosphonium chloride (TPPC) nanoparticles and PVDF mixture to make the filament for FDM printing. In this method, the TPPC powder and PVDF pellets were first mixed in the solid state and then melted at 190 °C while the mixing process continued for 10 minutes. The solidified mixture was then torn into small pieces and fed into an extrusion for making the filament with a diameter of 1.75 mm. Samples with 0 to 5 wt% of TPPC were fabricated in a multi-layer grid changing the print direction in each layer by 90° with respect to the previous layer. The measured accumulated β- and γ-phase contents in the crystalline form of the prepared samples showed an increase from 28.9% to 83.8% with 0 and 5 wt% of TPPC, respectively. The enhanced β-phase formation in the presence of TPPC is explained by ion-dipole interactions, which were also reported by Liu et al. [63]. The authors explained that the interaction between the phosphorus atom with a positive charge and the PVDF dipole (CH_2-CF_2) could exceed the energy required for the transformation from the α- to β-phase. The shear force applied to the molten material exiting the nozzle during printing is also believed to enhance the crystallization orientation. The mechanical properties of the samples also showed that the compression modulus and maximum stress for the samples decreased with a higher content of TPPC. The authors considered this as an improvement in the flexibility of the samples with higher TPPC content, which could increase the piezoelectric response in energy harvesting applications. The maximum open-circuit voltage of 6.62 V and short-circuit current of 87.6 nA were reported for the sample with 5% of TPPC, while the sample with 0% of TPPC generated 1.25 V.

Chen et al. [65] used a PVDF-based solution and ink printing method to manufac-

ture thin films with a thickness of 40 μm. The solution was prepared in a multi-step procedure by dissolving PVDF (12-17 wt%) in DMF and adding multi-walled carbon nanotubes or graphene (0.03 wt%) as conductive nanoparticles. The samples were then printed by ejecting the inks with various combinations of the components from a syringe with a 0.33 mm outer diameter needle while applying an electrical potential difference (3 kV and 6 kV) between the needle and the printing bed. As results showed, higher content of PVDF in the solution improved the crystallinity of the sample. However, above 20 wt%, the adhesion to the printer bed deteriorated, and the mechanical stretching factor became less effective. The stronger applied external electric field between the needle and the bed also increased the crystallinity from 36% to 56%. By keeping the PVDF content fixed at 15 wt% and the external electrical potential at 6 kV, the introduction of both graphene and multi-walled carbon nanotubes enhanced the crystallinity and β-phase content. However, the graphene additive created higher crystallinity (78%) compared to multi-walled carbon nanotubes (62%). The piezoelectric coefficient, d_{33}, for the samples with 15 wt% of PVDF and printing under 6 kV were reported as -2.3, -5.5, and -8.7 pC/N for pure PVDF, PVDF with multi-walled carbon nanotubes, and PVDF with graphene, respectively.

Table 2.1: Key aspects of FDM and inkjet 3D printing methods for manufacturing of piezoelectric polymers

Material	**Method**	**Poling condition**	**Reported piezoelectricity**	**Reference**
PVDF	FDM	EPAM	NA	Lee and Tarbutton [3]
PVDF	FDM	NA	d_{31}=1.19 pm/V	Porter et al. [59]
PVDF	FDM	Corona poling	d_{31}=4.8 $\times 10^{-2}$ pC/N	Kim et al. [60]
PVDF-TrFE	Self-made printer	Corona poling	d_{33}=130 pC/N (6 layered sample)	Yuan et al. [61]
PVDF	FDM	EPAM	d_{33}=0.66 pC/N (1 layer) d_{33}=0.23 pC/N (2 layer)	Tarbutton et al. [62]
PVDF + ionic liquid	FDM	NA	NA	Liu et al. [63]
PVDF + TPPC	FDM	NA	NA	Pei et al. [64]
PVDF PVDF + carbon nanotubes PVDF + graphene	Ink printing	NA	d_{33}=2.3 pC/N d_{33}=5.5 pC/N d_{33}=8.7 pC/N	Chen et al. [65]

CHAPTER 3: EXPERIMENTAL DESIGN AND METHODOLOGY

An iterative approach was adopted to refine the research methodology for this dissertation. With each iteration, adjustments were made based on the findings from the previous version, aiming to enhance the overall methodology.

As described in the literature review section, Lee and Tarbutton [3] claimed to manufacture samples that were piezoelectric via EPAM method. As the continuation of their work and with the goal to manufacture multi-layer samples, new samples were 3D printed using EPAM. However, no response could be obtained from the samples. In order to determine the source of the problem, the following steps were performed:

First, it was necessary to ensure that the performance of the EPAM was not affected in any way by the material properties of different grades of PVDF. Therefore, PVDF from Arkema (under the brand name of Kynar) and Solvay (under the brand name of Solef) were used for sample preparation. As it is described in the next chapter, XRD results and piezoelectric response measurements confirm that the samples were almost completely in non-polar α -phase which explains the absence of piezoelectric response in the samples.

Second, To prevent early electrical breakdowns, the printing and poling processes were separated. Also, it was tried to apply higher electric fields to the printed samples in a post-process step. For this purpose, high voltages were initially applied directly to the sample's surfaces, known as direct poling. For direct poling, both surfaces of the samples had to be covered with a conductive material (electrodes). The first option was commercial copper tapes with one-side adhesive. Due to the rugged surface of 3D printed samples, copper tape had poor surface adhesion. Next, metal electrode

sputtering was used to achieve great adhesion and cover any voids and dents on the surface that are not accessible with copper tape. Denton Desk IV Sputter was used to deposit a thin layer of gold (50 nm) as an electrode on the surface of the samples. Nevertheless, sputtering involves creating plasma in a vacuum, which requires specialized systems, increasing the overall process' complexity which is opposite to the main goal of this research of using additive manufacturing as a simple single-step procedure for fabricating piezoelectric devices.

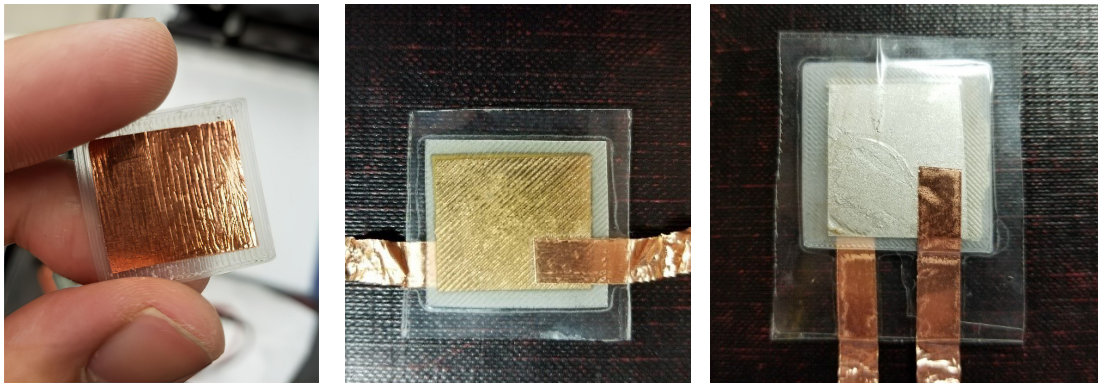

(a) (b) (c)

Figure 3.1: PVDF samples with different type of electrodes: copper tape (a), sputtered gold (b) and silver paint (c).

Conversely, conductive paint was very effective at adhering to surfaces as well as covering small voids. Copper paint and silver paint purchased from MG Chemical produced similar results, but silver paint had the edge by forming smooth, hard, and abrasion-resistant electrodes. Because of its good adhesion, high conductivity, and ability to be applied with spray guns, silver paint became the main material as the electrode for latest samples. Table 3.1 lists the properties of the silver paint.

To apply high electric fields, Matsusada EQ30P1 unipolar (positive) 30 kV DC power supply was used. Initially, direct poling was performed in the air, and the maximum achievable voltage was found to be around the threshold that the breakdown occurred (9 kV) in EPAM method. Also, the samples were immersed in silicon

Table 3.1: Electrical and chemical properties of the conductive silver paint form MG chemical.

Resistivity	Surface Resistance @ 50 μm	Cure Time	Service Temperature
$1.0 \times 10^{-4}\ \Omega \cdot cm$	0.015 Ω/sq	24 h @ 22 °C 30 min @ 65 °C	-40 to 120 °C

oil which has very high dielectric strength, to increase the magnitude of the high voltage, but there was no significant improvement in the poling process since electrical breakdown occurred at 10-11 kV.

As an alternative to direct poling, corona discharge method was also used. Using this method, which will be discussed in more detail later, you can create higher electric fields with a lower possibility of breakdowns occurring. The Corona discharge method uses a high voltage to ionize the air close to the needle tip and direct the resultant ions/charges to the surface of the sample placed under the needle (see Figure 3.2).

Based on X-ray Diffractometry (XRD) analysis whose results are presented in the next chapter, further poling in a post-process step did not result in any noticeable polar phase formation, since the samples were still in α-phase. This is in accordance with the fact that PVDF cooling down from melt (the main process in the FDM method) to alpha phase is a thermodynamically favorable process due to the lowest potential energy. Therefore, as a preliminary result, it was found that pure PVDF may not be suitable for additive manufacturing piezoelectric devices using FDM. This outcome resulted in replacing PVDF with its well-studied copolymer, PVDF-TrFE. As mentioned in the previous chapter, the incorporation of TrFE units into the PVDF chain disrupts the regularity of the molecular structure, making it more difficult for the copolymer to adopt the tightly packed α-phase conformation. As a

result, the copolymer favors the β-phase conformation upon cooling from the melt. This is because the TrFE units introduce steric hindrance and reduce the crystallization temperature of the copolymer compared to pure PVDF, thereby promoting the formation of the β-phase.

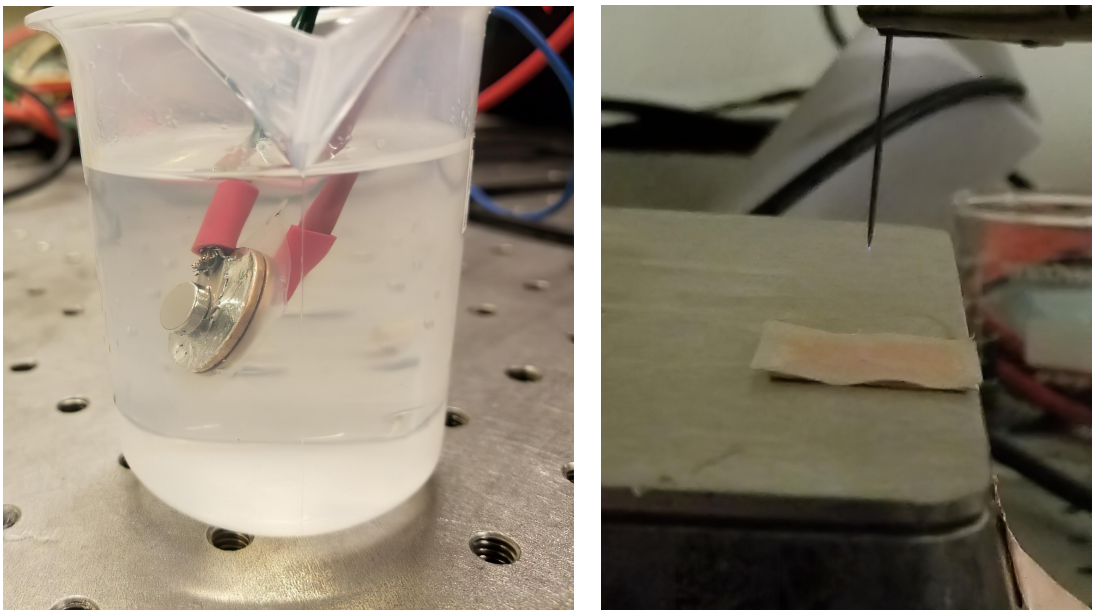

(a) (b)

Figure 3.2: The experimental setups for direct poling in silicon oil (a) and corona poling under a needle and on a hot plate (b). For direct poling, samples were sandwiched between two metal disks and immersed in silicon oil.

PVDF-TrFE is only available in the form of powder and therefore needs to be converted into filament to be used in FDM method. Two batches of powder PVDF-TrFE with 20 mole% and 25 mole% TrFE (500 and 100 gr respectively) were purchased from Solvay in powder form which the properties are listed in Table 3.2. Since we were the first team to use PVDF-TrFE in FDM 3D printing, the filament extrusion parameters such as heaters temperature and extrusion speed, needed to be found to obtain the filament with high consistency in diameter (1.75 mm) and free of defects like bubbles.

The NEXT 1.0 filament extruder by 3Devo, was chosen for this purpose due to its

Table 3.2: Properties of PVDF-TrFE purchased from Solvay

TrFE Mole%	Melting Point (°C)	Curie Temperature (°C)	d_{33} (pC/N)
20%	145	133	-25
25%	146	116	-24

advanced extrusion parameters control. This extruder uses 3 heating zones and an optical sensor to detect filament diameter in real time so it can modify the extrusion rate accordingly. As PVDF-TrFE and PVDF have very close melting temperature, and because of much lower cost of PVDF, the filament extruder was first calibrated with PVDF to make filament with 1.75 mm thickness. The optimal temperatures of the heater zones for extruding PVDF-TrFE were found to be 195 °C (closest to the hopper), 210 °C (middle heater) and 200 °C (closes to the nozzle). The rotating speed of the worm gear which pushes the powder into the heater, was also set to 6rpm.

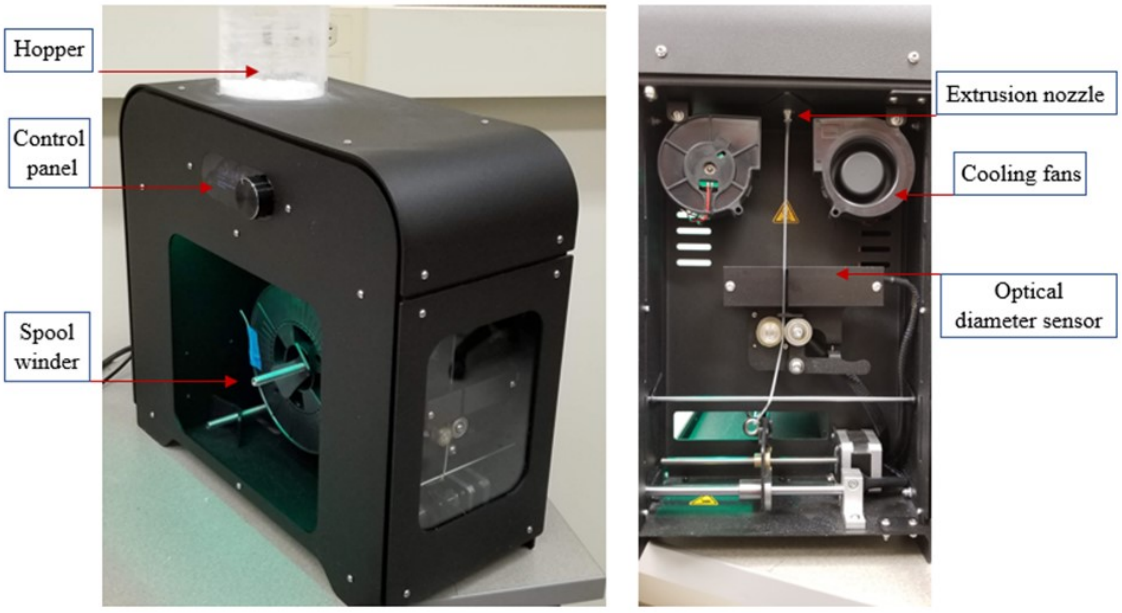

Figure 3.3: NEXT 1.0 filament extruder

3.1 Printing

Prusa MK2, an FDM printer with no enclosure was selected for printing PVDF-TrFE samples. As explained in the previous chapter, the path of the extrusion nozzle and other printing parameters are defined and performed by the printer via the g-code that is generated in a software called slicer that slices the CAD model of the part into thin layers. Slic3r, an open-source software, was used for this purpose and the generated g-code was then imported to Pronterface, the software for controlling the printer. The print parameters such as print speed, extrusion width, and infill angle were set in the slicing step. It was challenging to find the optimum print settings with minimal trial and error since there were no available reported print settings for PVDF-TrFE. Therefore, the print settings had to be tweaked to obtain the best quality for the samples. Furthermore, since PVDF-TrFE had the tendency to peel off the bed due to low adhesion, a thin layer of paper glue or a small amount of hair spray with PVA was used to improve the adhesion.

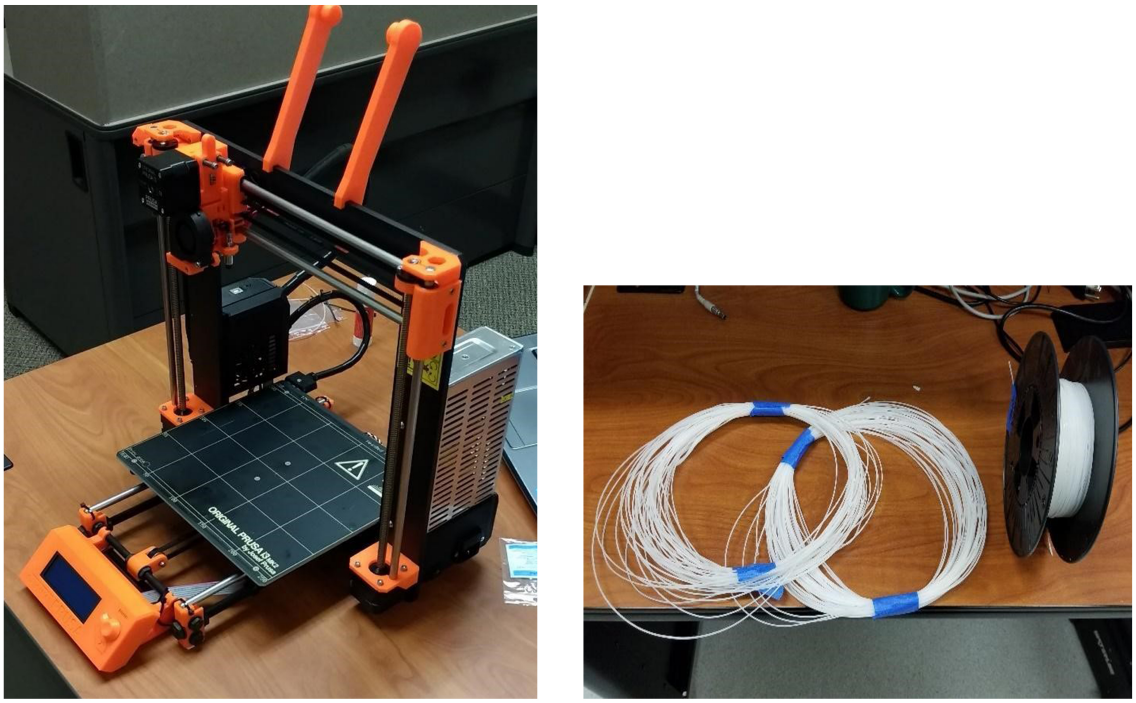

(a) (b)

Figure 3.4: Prusa MK2 printer (a) and the prepared PVDF-TrFE filament (b).

The print quality is the most important factor from the standpoint of structural strength and more importantly for poling process. If samples have many voids and defects, poling process would not be possible due to early electrical breakdown which results in destroying the electric field required for aligning dipoles in the samples. The most important print settings found to have the highest effect on the print quality and the corresponding tuning range that resulted in the best print quality are presented in Table 3.3.

The dimensions of the single-layer samples were selected to be $35 \times 35 \times 0.3$ mm (length $\times$ width $\times$ thickness). By visually inspecting the samples, the ones with no visible defects (gaps, cracks, and holes) were selected to be poled. It was also found that the samples printed with an infill angle of 45° tolerate large deformations like bending in random directions better than the ones printed with 0° or 90°. A separate set of samples with two layers and an overall thickness of 400 mm (shown in

Table 3.3: Printing settings range found to result in the best sample quality.

Extrusion Temp (°C)	Bed Temp (°C)	Print speed (mm/s)	Nozzle diameter (mm)	Filament diameter (mm)
220-230	50-100	10-30	0.2-0.4	1.75

Figure 3.7) were also printed to investigate how printing in multiple thin layers rather than one thick layer affects print quality, the highest achievable corona voltage, and piezoelectric response. Compared to the first layer, the second layer's infill angle was 90° out of phase.

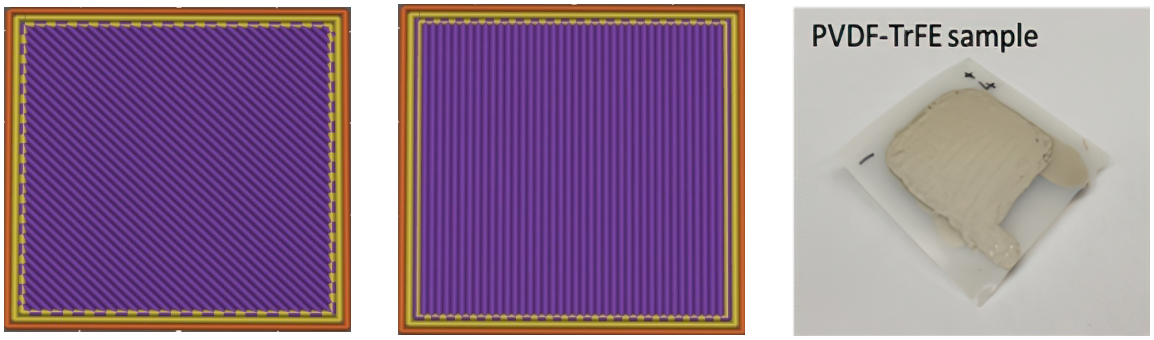

(a) (b) (c)

Figure 3.5: The CAD modeled samples sliced with the infill angle of 45° (a), 90° (b), and 3D printed sing layer PVDF-TrFE sample with silver paint on both sides as electrodes (c).

Furthermore, to study the structural approach to induce higher stress in the samples [17, 66, 67], a double-layer sample with one piezoactive layer (PVDF-TrFE) and the other layer as a non-piezoactive substrate (PVDF) was designed and printed. The sample preparation procedure is illustrated in Figure 3.6. Since PVDF-TrFE showed better adhesion to the printer bed than PVDF covered with silver paint, printing PVDF-TrFE as the first layer resulted in better overall sample quality. The silver paint thin layer dried out almost immediately after applying due to the high

temperature of the printer bed.

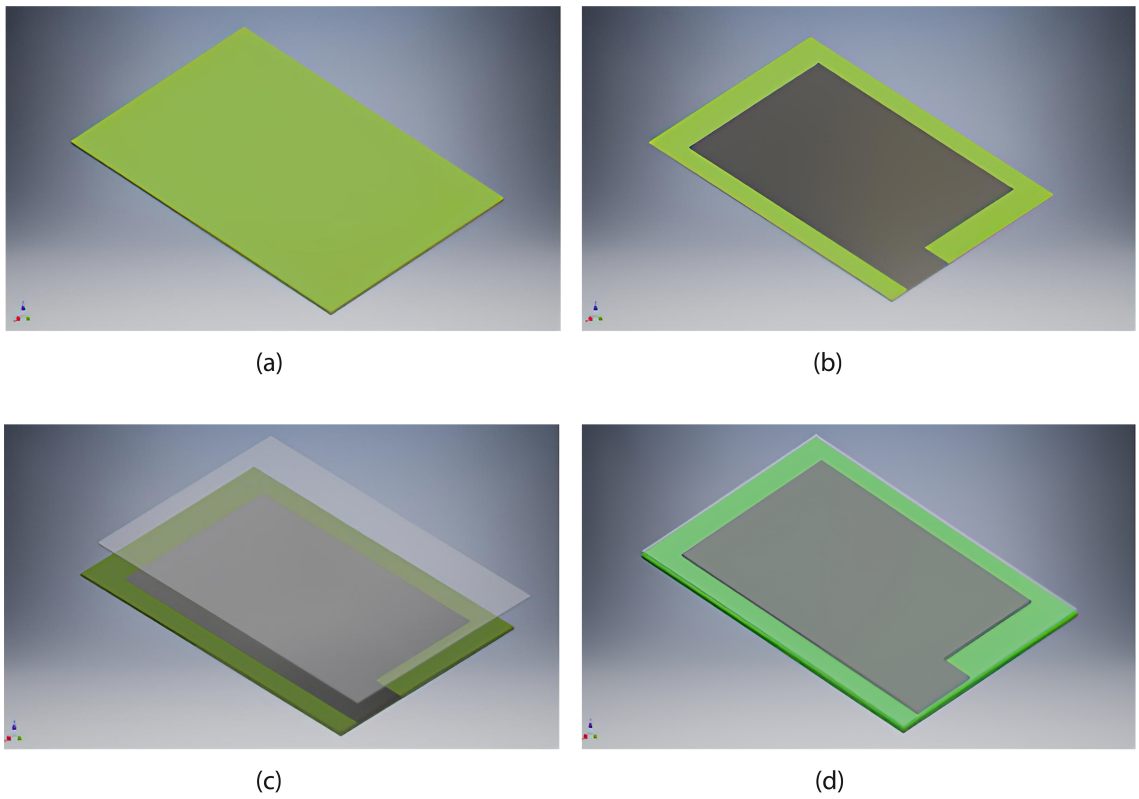

Figure 3.6: Schematic of 3D printing steps of the sample with one piezoelectric layer on top of a substrate: PVDF-TrFE (green) as active piezoelectric layer(a), silver paint layer (gray) as electrode (b), PVDF (transparent) as substrate (c), and the complete sample (d).

PVDF-TrFE was also successfully printed as the second layer on top of a PLA layer which was covered with silver paint. Although this sample was not used for further poling, the good adhesion between the PVDF-TrFE and PLA indicates the possibility of printing multi-material complex geometry.

(a) (b) (c)

Figure 3.7: Double layer PVDF-TrFE (a), single layer samples with sputtered gold electrode cut from 35×35 mm samples (b), and the prepared double layer sample with one piezoactive layer (PVDF-TrFE) and with silver paint electrode (c).

The prepared PVDF-TrFE samples were then analyzed with XRD prior to poling process to determine their crystalline phase structure. To align the dipoles in the samples and make them piezoelectric, a high electric field was applied. Based on the preliminary results, in contrast to direct poling, corona poling showed much more promising and repeatable results and therefore, all the samples were poled only with this method. In the next section, this poling method is explained in more detail.

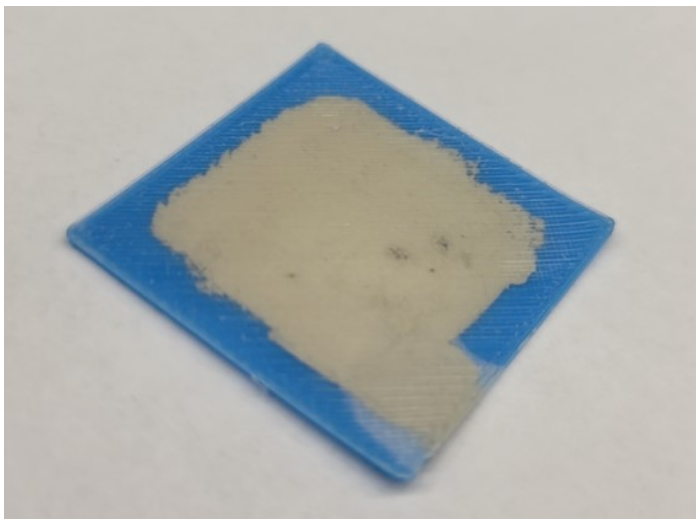

Figure 3.8: The sample with one layer of PVDF-TrFE printed on top of a PLA substrate with silver paint in between.

Filament extrusion and printing PVDF-TrFE required trial and error to obtain samples with good print quality to be free of defects (voids, gaps, etc.). As PVDF-TrFE is more expensive (Solvene with 20 mole% TrFE priced $5175.0 for 1 kg in 2018), the number of these trials and errors is basically very limited. On the other hand, PVDF-TrFE has never been extruded into filament for the purpose of 3D printing before this work, which made finding the optimum settings more challenging.

The ideal filament was expected to have a circular cross-section with a 1.75 mm diameter. However, there are many sources of uncertainty that resulted in imperfections in the extruded filament. During the filament extrusion process with the NEXT 1.0 extruder, the puller system pulls the cooled-down filament. If the filament was still hot and therefore soft, the forces applied to it during the pulling step could cause the filament cross-section to become more oval rather than circular. This could later result in the wrong measurement of the diameter by the optical sensor, which controls the extrusion rate. One solution to this issue was to reduce the extrusion temperature as much as possible to accordingly decrease the temperature of the extruded filament. However, lowering the extrusion temperature by more than 200 °C increases the required torque for the extrusion screw, which stalled the motor in some cases. Therefore, the last heating zone temperature (closest to the extrusion nozzle) had to be 200 °C or more. Changing the first and the second heating zone temperatures did not have a noticeable effect on this issue. Also, another observed issue was the existence of air bubbles in the filament (see Figure 3.9). This was first observed in the purchased off-the-shelf PVDF filament. However, this issue was not detected in PVDF-TrFE filament made in the lab.

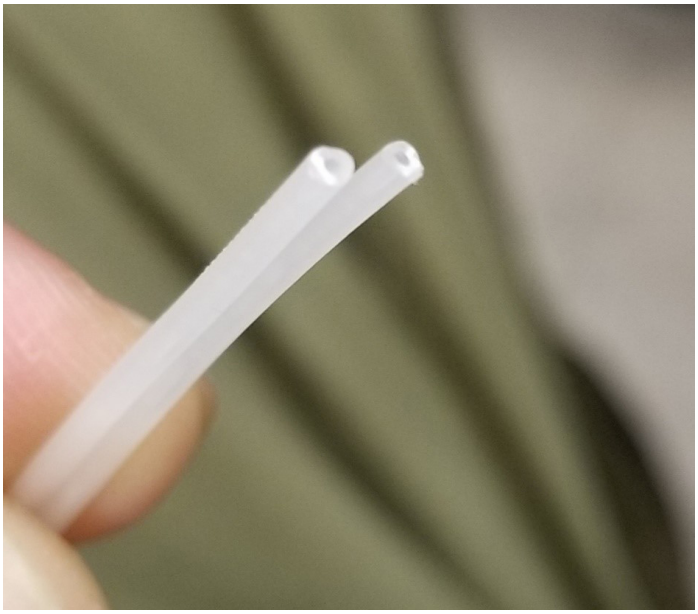

Figure 3.9: Air bubble found in the purchased commercial PVDF filament.

The quality of the prepared filament hugely affected the print quality. The generated g-code that contains the extrusion rate for the prints, is based on constant and ideally 1.75 mm filament. Therefore, the smallest deviation in the filament diameter could result in extrusion of either less or more than the nominal amount of material, which created gaps or blobs. This issue normally was followed by a clogged nozzle. It is important to note that there might be more than a single reason for the prints to fail. For example, in the two cases that are illustrated in Figure 3.10, other reasons such as nozzle height and filament feeding system fault also contributed as well. To mitigate the effect of the variations in filament diameter, this parameter is required to be updated frequently in the print settings.

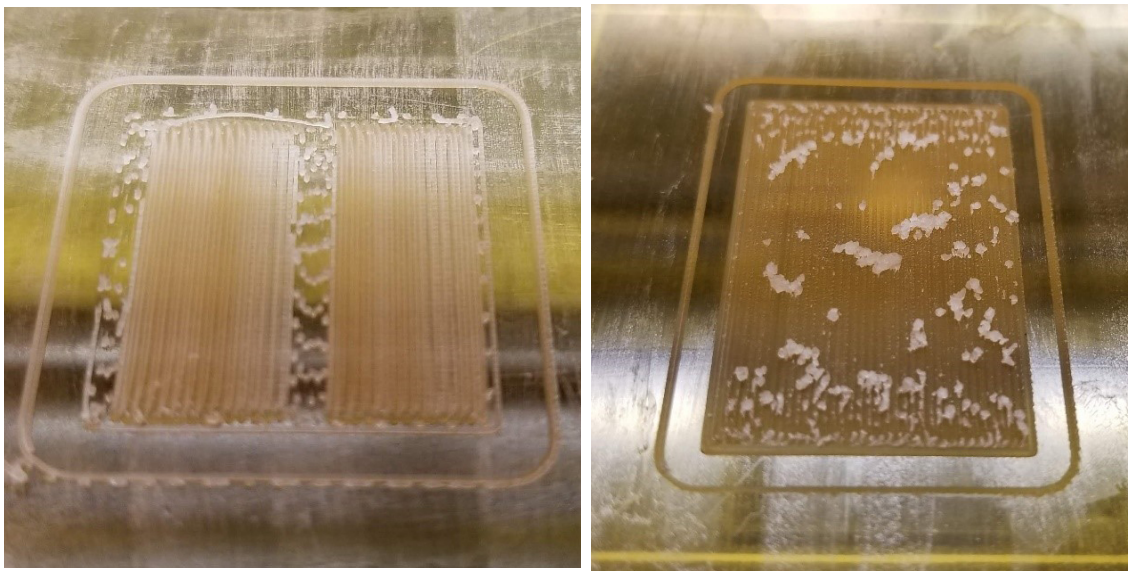

(a) (b)

Figure 3.10: : Print failure due to less than required extrusion rate (a) and excessive extrusion rate (b).

3.2 Corona Poling

Corona discharge method has been used widely for charging the surface of materials with the applications of electrophotography, electrets, polymers, etc. The simplest design consists of a point electrode or fine wire as ionizer/emitter part and a plate or cylinder as the receiver of the ions. In this design, controlling the charge uniformity is difficult and therefore a grid with the same polarity of the point is normally used between the point and the plate to control these parameters [68].

Corona occurs as the result of ionization of the gas near the emitter due to a high electric field. The ions then accelerate toward the low field plate. Positive and negative corona follow different regimes. By increasing the voltage, positive corona becomes a continuous glow while the negative corona goes to Trichel pulses regime [68]. At higher voltages, both types will experience streamer until breakdown occurs.

According to Warburg law [69], the current density in point-to-plane unipolar corona is distributed over the plane as: $\mathrm{J}(\theta) = J_0 \cos^5(\theta)\ and (J_0 \approx \frac{I}{2d^2})$ where I

is the total corona current and d is the gap length. It is observed that the distribution goes to zero at $\theta > 65°$. It is also shown that the maximum possible current at a given voltage U_0, $I_{sat} \sim \frac{2\mu\epsilon_0 U_0^2}{d}$ and for air at atmospheric density I_{sat} (μA) $\sim 4U_0^2$ (kV^2)/d (mm).

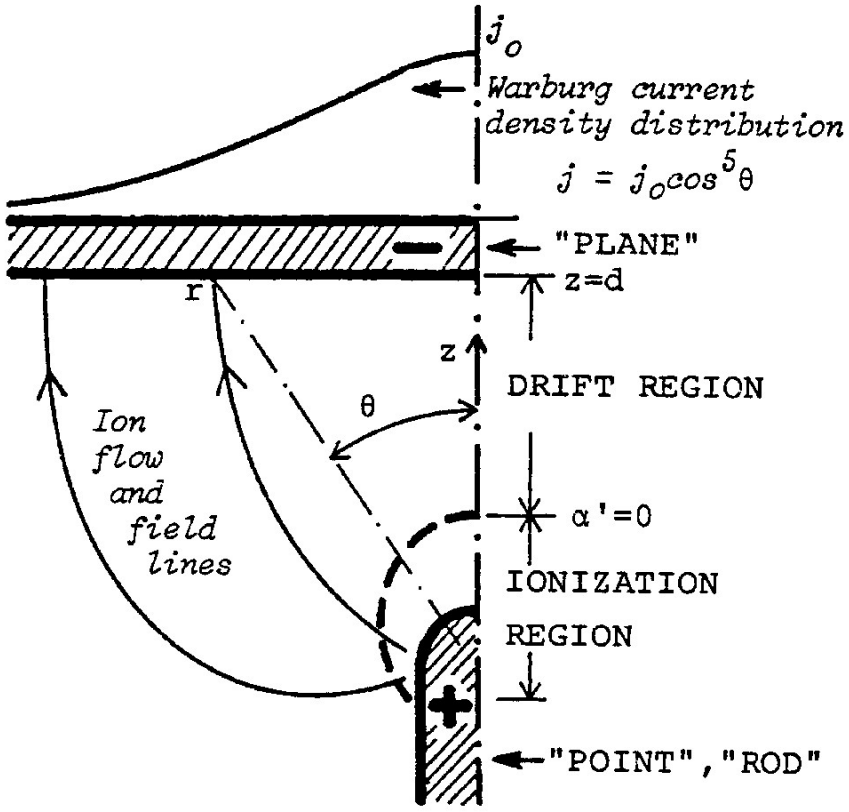

Figure 3.11: Corona discharge regions and ion flow pattern. Image taken from [69].

The ions generated in corona charging depend on the gas. In the air, positive corona mainly produces hydrated ions in the form of $(H_2O)_n H^+$, where n depends on the humidity of the air. In low humidity, the dominant ions are $(H_2O)_n NO^+$ and $(H_2O)_n (NO_2)^+$. For negative corona, the most important ion is CO_3^-, and in 50% humidity, approximately 10% of ions are $(H_2O)_n (CO_3)^-$ [68].

Streamer conduction corona occurs in the positive corona and at high currents. When the ion creation rate exceeds the absorption rate at the point electrode, a conductive plasma channel grows towards the plate electrode with a velocity of $106 m/s$

(in the air). This channel can be eliminated through electron attachment or transformed into a thermally ionized spark channel. In the latter case, ions with energies greater than 100 eV strike the surface, resulting in a different thermal energy influx compared to unipolar current coronas. Corona wind is another phenomenon in which the ions traverse from the point electrode to the plate electrode, their energy is transferred to the neutral gas molecules. A very strong gas flow carrying neutral and activated species toward the plate and impose heat and chemically excited atoms and molecules on it [69].

An electrode is not necessary for Corona poling, as opposed to Direct poling. Corona discharge is better suited for implementation alongside other manufacturing processes due to its advantages over direct poling. Poling the samples was accomplished with a needle-plate corona setup. A PVC tube was used as an enclosure for the poling station, which, according to [68], acts as a lens and directs the charges to the surface. Corona discharge was initiated by applying a high voltage with positive polarity (Matsusada EQ30P1) to the needle and grounding the bottom conductive surface. It is important to note that with the presence of the PVC tube, the corona discharge did not start properly.

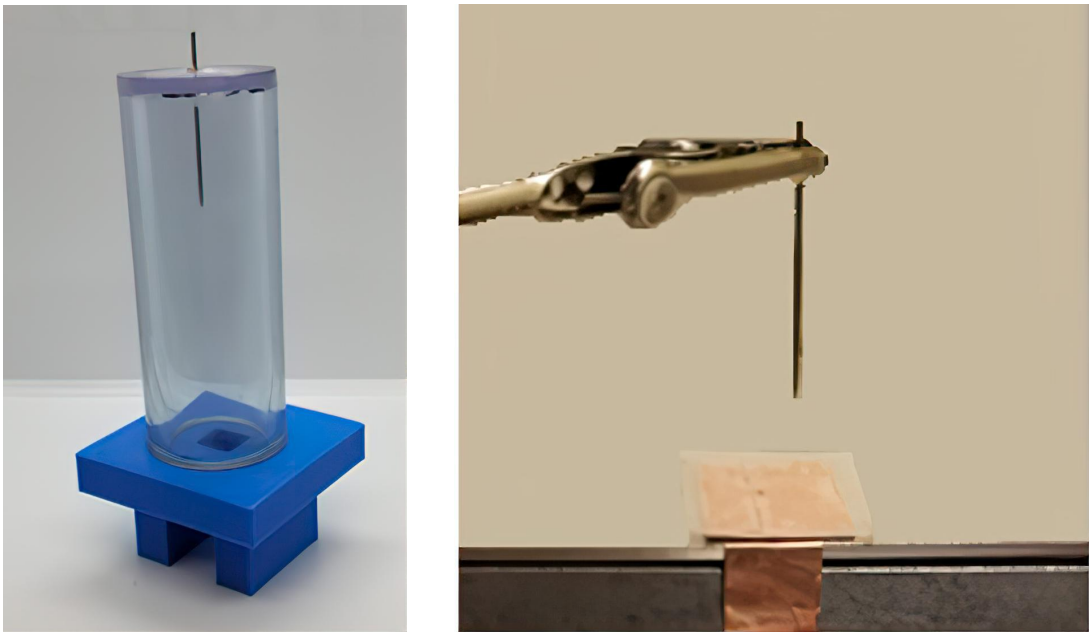

(a) (b)

Figure 3.12: Corona station with PVC tube (left), and needle-plate setup with sample placed on a copper plate over the hot bed (right).

The samples were placed on a copper plate (grounded electrode) for about 5 minutes at 80°C on a hot plate while the distance between the needle and the sample was set to almost 40 mm while 13-15 kV were applied to the needle. One issue with the simple point-plate corona poling setup shown in Figure 3.8 was that the generated charges and charged particles due to air ionization could travel to the area around the poling station and therefore become problematic for existing electronics. Hence, a new poling station was designed (Figure 3.13) to mitigate the mobility of charged particles and ions to the surroundings.

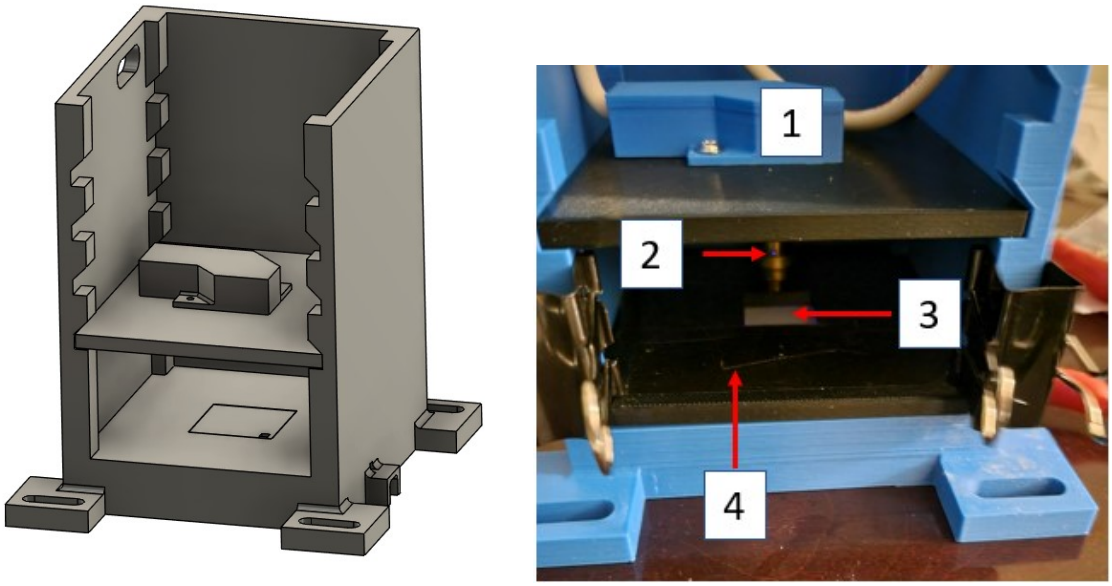

(a) (b)

Figure 3.13: Improved design of corona poling station to minimize the charge escape. (1) high voltage connector shield, (2) holder for a spring under compressing between the top and bottom black plates, (3) an opening in the bottom plate that the sample is placed under it on a grounded electrode, and (4) the bottom plate which holds the sample flat on the grounded electrode.

To prevent the charges from escaping to the ground electrode and help build up the charge on the sample, a cover with a 20×20 mm opening was placed on the sample (see Figure 3.11). However, there were still different issues with keeping the charges on the top surface of the sample, which will be discussed later. To minimize charge escape, the edges of the samples were covered with a thick layer (4 mm) of PVC tape. A set of experiments was designed to investigate the effect of the main corona poling parameters: corona voltage, duration, and needle-to-sample distance. The corona poling was performed at room temperature for 30 seconds to 10 minutes, with the needle voltage set up to 25 kV.

3.3 Material Characterization

X-ray Diffractometry (XRD) is an analytical non-destructive technique widely used in material science, geology, chemistry, and various other fields to investigate the crystallographic structure of materials. The basic principle behind XRD involves the interaction of X-rays with the atoms in a crystalline material. When X-rays strike the crystal lattice, they are scattered by the atoms, and the resulting diffraction pattern contains information about the arrangement of atoms in the crystal. According to Bragg's law, the diffracted X-ray is measured in the receiver and the sample's structure properties are calculated. The XRD procedure is shown in 3.14. By analyzing the angles and intensities of the diffracted X-rays, the lattice parameters, crystal phases, and crystallographic orientation of the sample can be determined. To determine the phase of the additive manufactured PVDF and PVDF-TrFE samples prior to and after electrical poling, PANalytical X'Pert Pro X-ray diffractometer with an X-ray source of Cu Kα line with the wavelength $\lambda = 1.54184$ Å(average) was implemented.

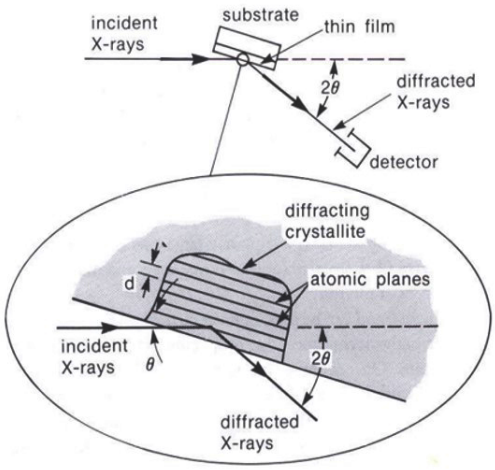

(a)

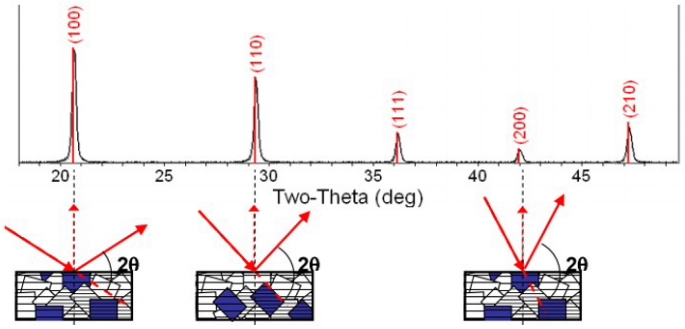

(b)

Figure 3.14: : Principle of XRD analysis (a) and plot of XRD for an example material (b). Graphs from graduate course Material Characterization (MEGR 8090) by Dr. Zhang.

CHAPTER 4: RESULTS AND DISCUSSION

This chapter presents the results of material characterization, piezo- and pyroelectric measurements. The piezoelectric response of the manufactured PVDF-TrFE samples was measured by applying normal load to the samples or deflecting the samples. The load and deflection were applied to the samples either manually (with a micrometer) or with a linear actuator. Also, as mentioned before, it is well known that PVDF-TrFE is both piezoelectric and pyroelectric, and therefore, if the samples were successfully poled, they had to create electrical charges when the thermal equilibrium of them was disrupted (pyroelectricity). Furthermore, additional tests were designed and conducted to investigate the effect of the corona poling parameters on the pyroelectric response.

4.1 X-ray Diffractometry Results

A single peak in the vicinity of 20° is a characteristic peak of the β-phase for PVDF-TrFE [45], which can be clearly seen in Figure 4.1(a). This characteristic peak was observed for all the 3D printed samples that were prepared from both batches of PVDF-TrFE (20% and 25%), indicating the existence of β-phase. The XRD analysis for PVDF samples is also provided in Figure 4.1(c), which suggests that only α-phase exists in all the PVDF samples independent of the grade or brand.

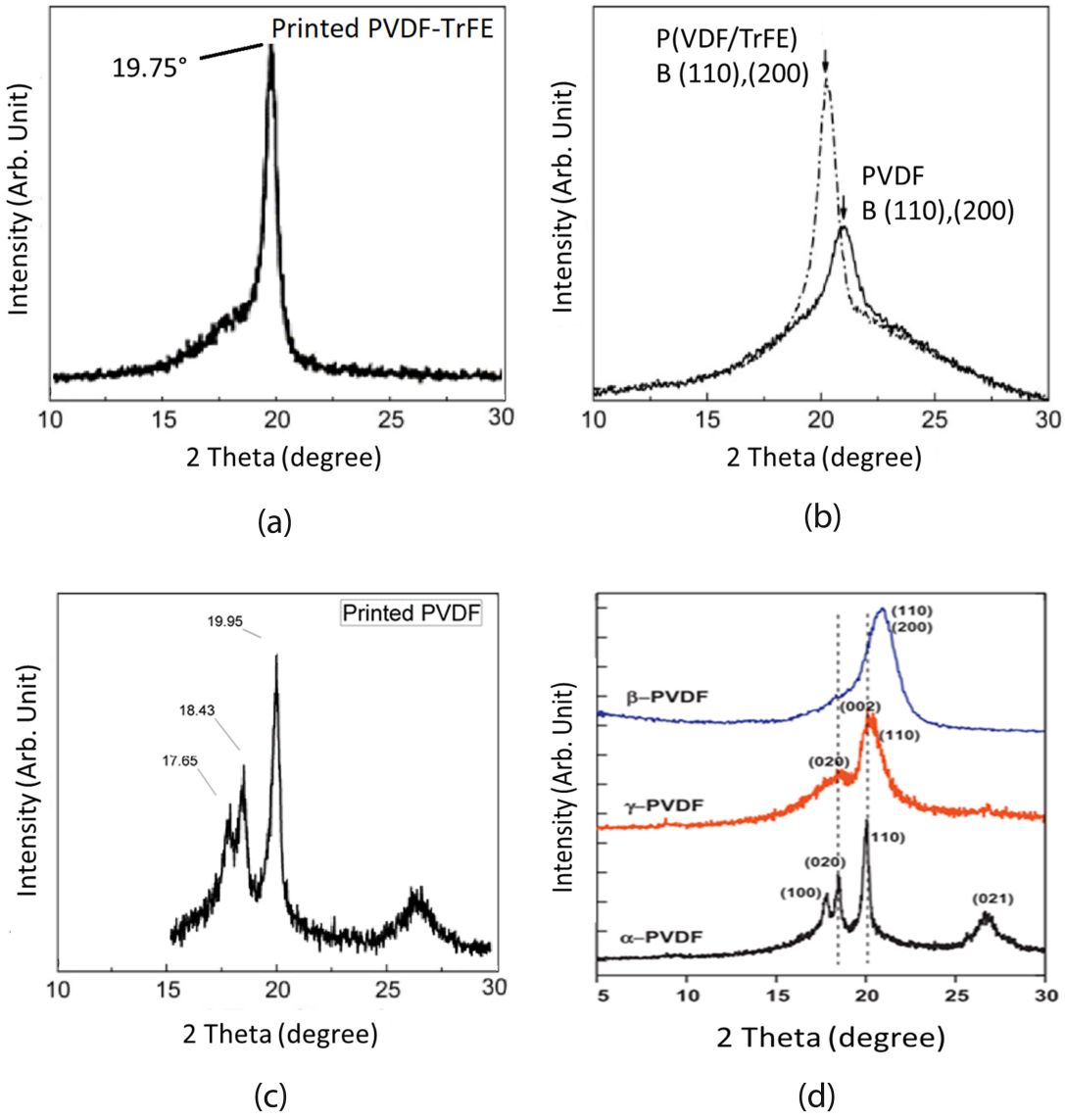

Figure 4.1: XRD graph of PVDF-TrFE 3D printed sample (a) and, the reported graph for beta phase (b) from [45], PVDF sample (c) and reported graph different phases of PVDF thin films (d) [21].

4.2 Piezoelectric Response

A BOSE ElectroForce 3200 tensile strength testing machine was used to test the PVDF-TrFE samples with gold electrodes (see Figure 4.6-middle). A copper block was mounted on the actuator of the tensile strength machine as the top electrode. The bottom brass electrode was placed on the load cell. The measurement setup was placed in a faraday cage to mitigate free electrical charges.

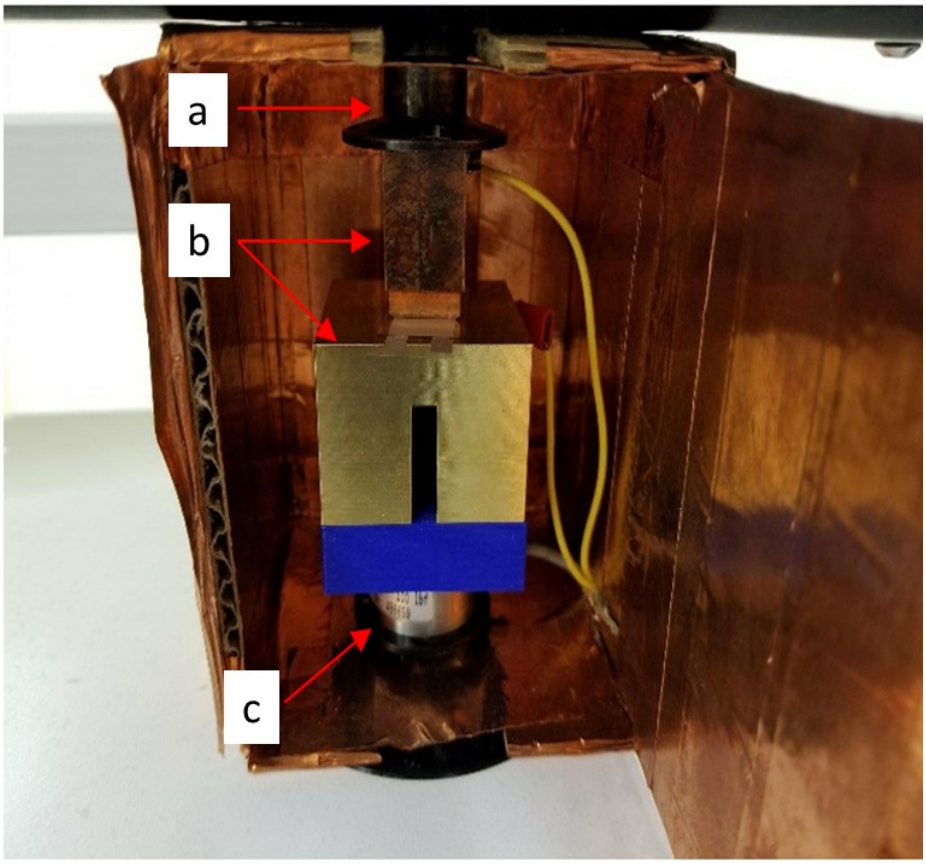

(a)

Figure 4.2: : Piezoelectric measurement setup in a Faraday cage installed on BOSE Electroforce. The normal load (static or cyclic) is applied via the actuator (a) to the sample placed between the top and bottom electrodes (b). The magnitude of the force is measured with the loadcell (c).

The generated electrical charges due to the piezoelectric response of the sample were measured with a Keithley 6517B electrometer and monitored via NI myDAQ using LabVIEW. A commercial sample from TE Connectivity (MEAS series) was also tested as the baseline. The result is illustrated in Figure 4.3. The asynchrony between the waveforms is due to applying and removing the force in the manual operating mode of BOSE ElectroForce. The response of the 3D printed sample was about 10% of the commercial sensor. The piezoelectric coefficients (d_{33}) were measured to be 22.5 pC/N and 2.5 pC/N for the commercial and 3D printed sensors, respectively. It is worth noting that due to the rough surface finish of the 3D printed PVDF-TrFE

sample compared to the commercial sample with a very smooth surface, the applied load could not be homogeneously distributed in the structure of the sample, which might contribute to its lower response.

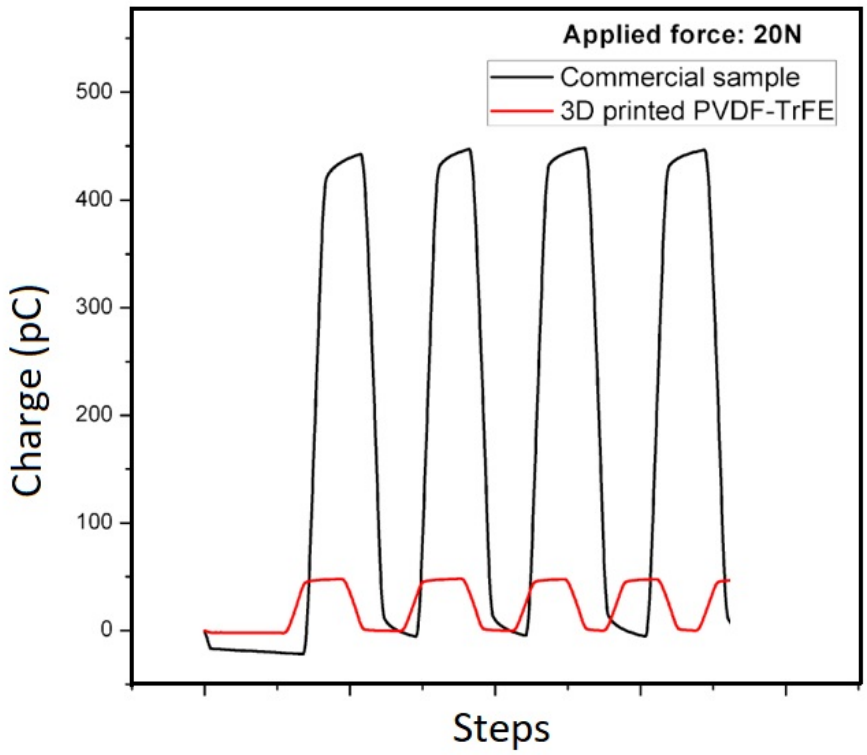

Figure 4.3: : Piezoelectric response of the 3D printed PVDF-TrFE sample (red) and commercial piezoelectric MEAS series sensor by TE (black), due to manually applied normal load of 20 N.

Deflection tests were also conducted on the samples to measure their response at high degree of deformation. For this purpose, one end of the single-layer sample was clamped in between two plates and deflected with a micrometer manually. In this setup, the sample was considered as a cantilever beam with one end fixed. The response of the sample due to 5 mm displacement of the free end is equal to 0.65 V (Figure 4.4). The step-like shape of the output signal is due to the intermittent displacement of the micrometer that was performed manually.

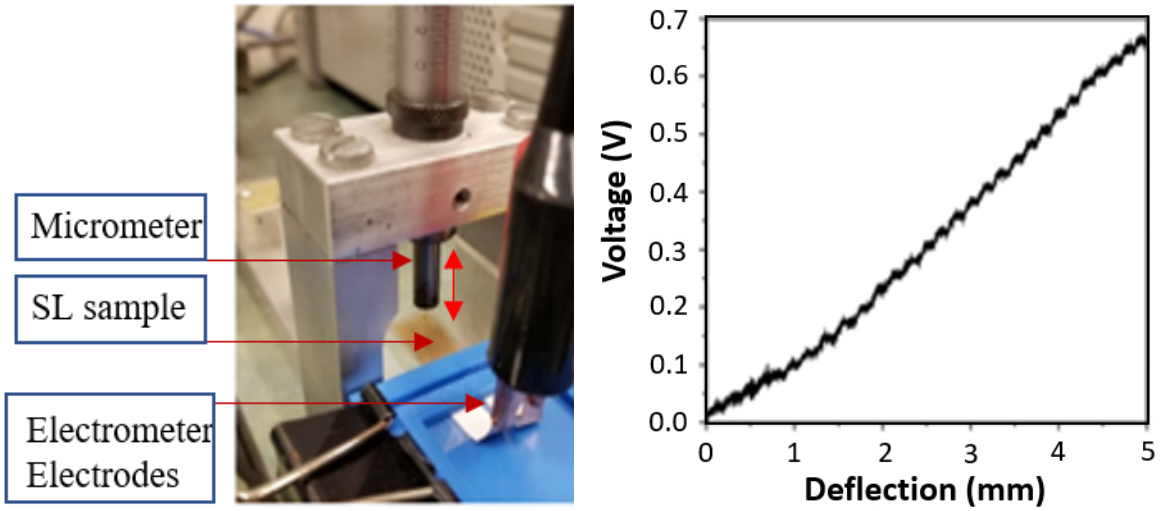

(a) (b)

Figure 4.4: The experimental setup for measuring the piezoelectric response of the single layer PVDF-TrFE sample due to deflection as a cantilever beam with one end fixed (a) and the corresponding response for 5 mm deflection of the free end.

The double-layer sample with PVDF-TrFE as the piezoactive layer on a PVDF substrate (Figure 3.7-right) was tested in deflection test under two conditions: 1)applying displacement to the middle of the sample with both ends free to slide (illustrated in Figure 4.5), and 2) deflecting one end of the sample while the other end was fixed (see Figure 4.6). Both tests were performed with BOSE ElectroForce and by applying precise cyclic displacement. Furthermore, the behavior of the sample in free vibration mode after an impact applied to the free end (by flicking) is shown in Figure 4.7. The sample was also modeled in Autodesk Inventor 2016 for stress analysis and determining the areas which experience more stress in every test. Like the test for the single-layer sample, the voltage difference between the electrodes was measured with Keithley 6517B electrometer and monitored in LabVIEW.

In the first test, the sample was placed under the actuator of the ElectroForce while preloaded to make sure that the sample was experiencing only bending (no impact effect). Then, 2 mm displacement in the form of 1 Hz sinewave was applied to the

center of the sample via the ElectroForce actuator. As illustrated in Figure 4.5, The measured response was ∼19 V peak-to-peak with high signal-to-noise ratio. Since the double-layer sample is thicker (∼450-500 μm) than the single-layer sample (∼300 μm), it is also stiffer and therefore for the same displacement larger stress appears in the sample which results in greater charge buildup on the electrodes. Also, the actuator was connected to the ground to eliminate any free charges during the measurement. Moreover, as explained before, a faraday cage was used to enclose the actuator and sample to mitigate the effect of free charges. The PVDF layer (bottom) behaves as an insulator and prevents external free charges to reach silver paint electrode that is sandwiched between the layers.

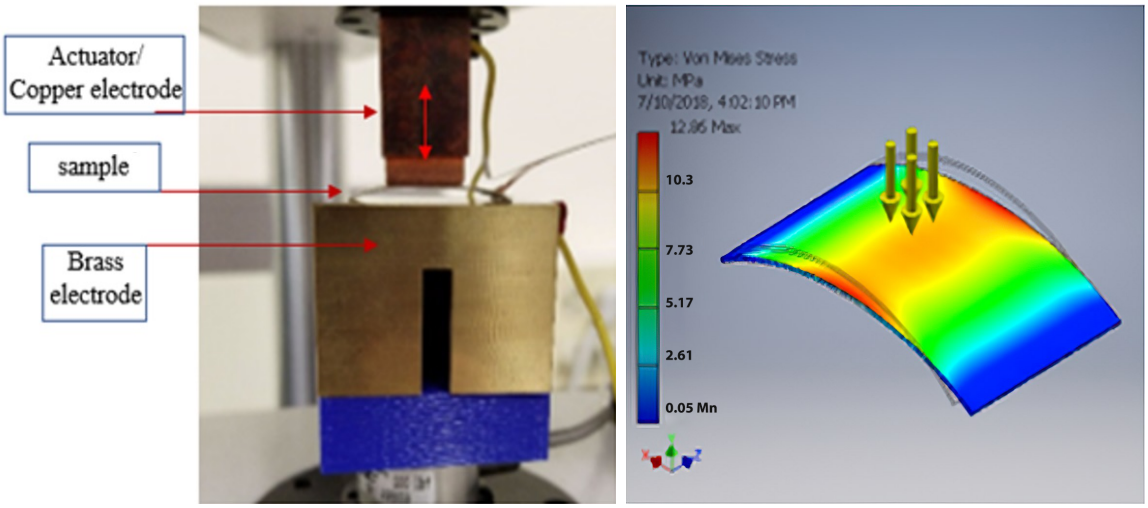

(a) (b)

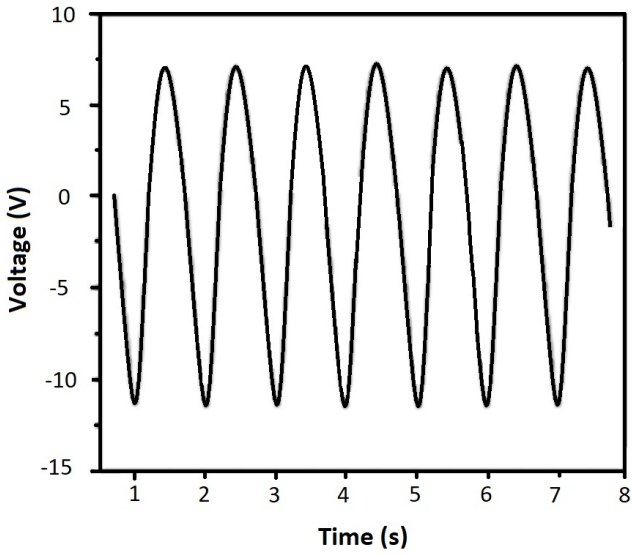

(c)

Figure 4.5: Piezoelectric response of the sample with a substrate to 2 mm displacement in bending mode. Measurement setup (a), Von Mises stress distribution (b), and the piezoelectric response of the sample (c).

Next, the sample was constrained in one end. The free end was subjected to a set of cyclic displacements which the properties are listed in Table 4 1. Here again, the sample was mounted in the setup under a small pre-applied displacement to ensure that the response is due to shear stress (bending mode) and not from any impact

Table 4.1: Properties of waveforms used for the sample with substrate in one free end cantilever model

Zone	**Waveform**	**Waveform Properties**
1	Sine	2 mm at 1 Hz for 10 cycles
2	Sine	1 mm at 1 Hz for 10 cycles
3	Sine	2 mm at 5 Hz for 10 cycles
4	Triangle	2 mm at 1 Hz for 10 cycles
5	Square	2 mm at 1 Hz for 10 cycles
6	Sine	2 mm at 20 Hz for 10 cycles

to the sample. The effect of pre-applied displacement to the sample can be seen in the first part of the response graph in Figure 4.6, where the signal drops down from 0 to -5 V. The increase in amplitude of the signal for square waveform (zone 5), despite a constant displacement, can be explained by very fast movement of actuator rather than a smooth movement that occurs during sinewave or triangle waveforms. Therefore, during the square waveform step, the sample was experiencing some impact too alongside bending.

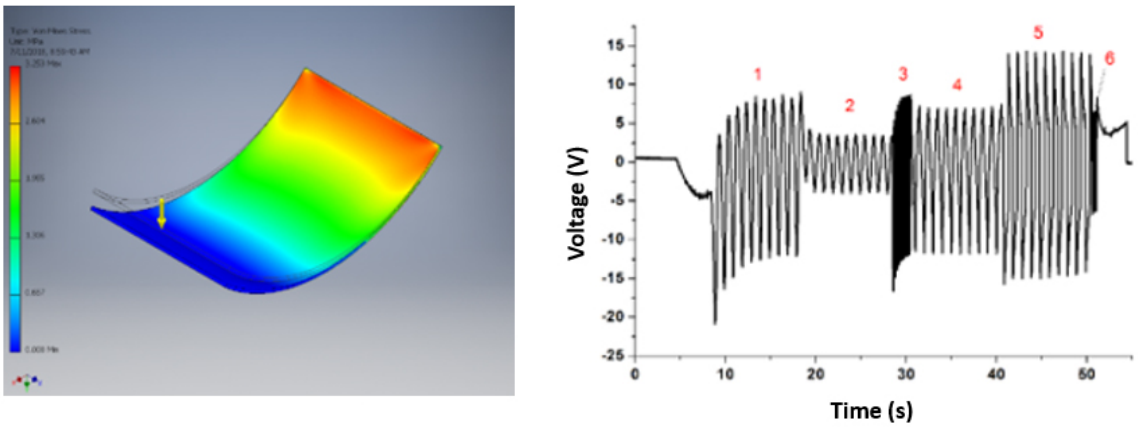

(a) (b)

Figure 4.6: Stress distribution in the sample with substrate to deflection at one end (a) and the piezoelectric response of the sample (b) corresponding to the input displacement listed in Table 2.

For testing the behavior of the sample in natural vibration mode, the sample was constrained in one end and got excited on the free end with an impact (flicking). Although the magnitude of the impact due to flicking is not measured but the response of the sample and its frequency response is clearly visible in Figure 4.7. The response of the sample in this test was measured to be 130 V peak to peak which was much higher compared to single-layer PVDF-TrFE samples. With the same setup, we observed only 3 V peak to peak for the single-layer sample. However, it should be mentioned that the area of the single-layer sample was almost half of the double-layer sample.

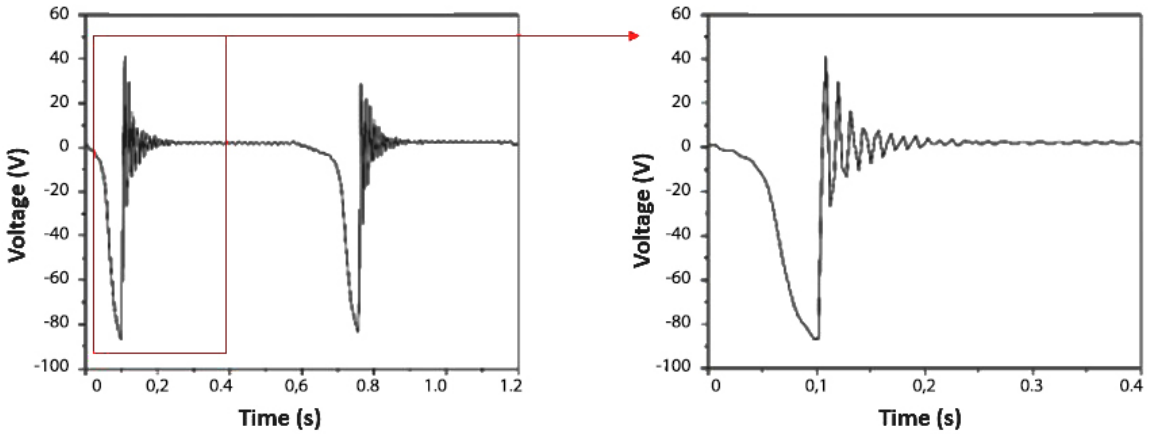

Figure 4.7: : Piezoelectric response of the double-layer sample (PVDF-TrFE on substrate) in free vibration mode after the free end was impacted by flicking.

All the results presented so far are for the samples which were poled under a simple needle-plate corona poling setup. After the new corona poling station was designed and built to better control the mobility of the created ions and charged particles during the poling process, a new batch of single layer PVDF-TrFE samples were prepared to systematically investigate the effect of poling parameters on the piezo- and pyroelectric response.

The piezoelectric response of one of the samples, which was poled under 19 kV for 5 minutes at room temperature with a needle-plate distance of 20 mm, was measured to be $\sim$ 25 V (see Figure 4.8). The noise amplitude was found to be $\sim$125 mV, resulting in a very high signal-to-noise ratio (about 200).

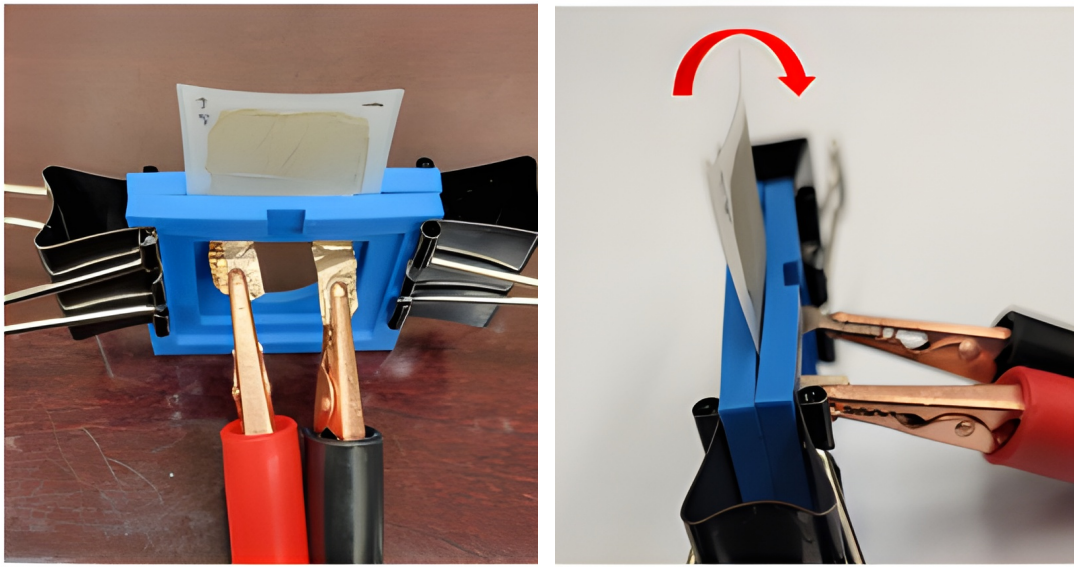

(a) (b)

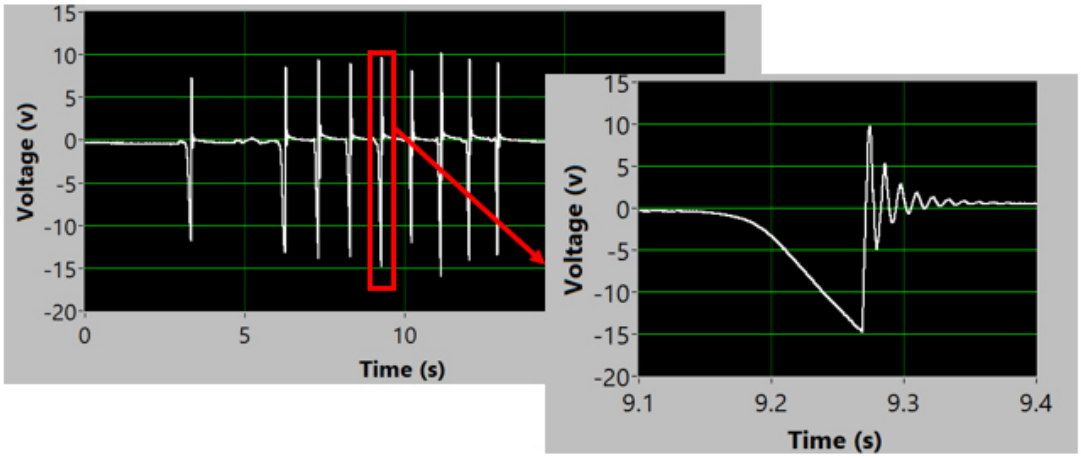

(c)

Figure 4.8: The piezoelectric response measurement setup for free vibration mode - front view (a) and side view (b). The sample was deflected without impacting the free end (no flicking) and released. The piezoelectric response (25 V peak to peak) of a single layer sample (c) poled in the corona poling station under 19 kV (with 20 mm needle-sample distance) for 5 minutes at room temperature.

4.3 Pyroelectric Response

To evaluate the pyroelectric response of the PVDF-TrFE samples, the PVDF-TrFE samples were illuminated by a 30 mW laser beam that was placed 30 mm away from

them. The radiation pressure applied to the samples was considered negligible. The initial tests were done with the laser continuously impinging on the sample and in 1- or 5-second intermittent shining modes. The results for the same sample poled under 19 kV (Figure 4.8) are shown in Figure 4.9. A low pass filter with cutoff frequency <20 Hz was used to eliminate the noise in the signals.

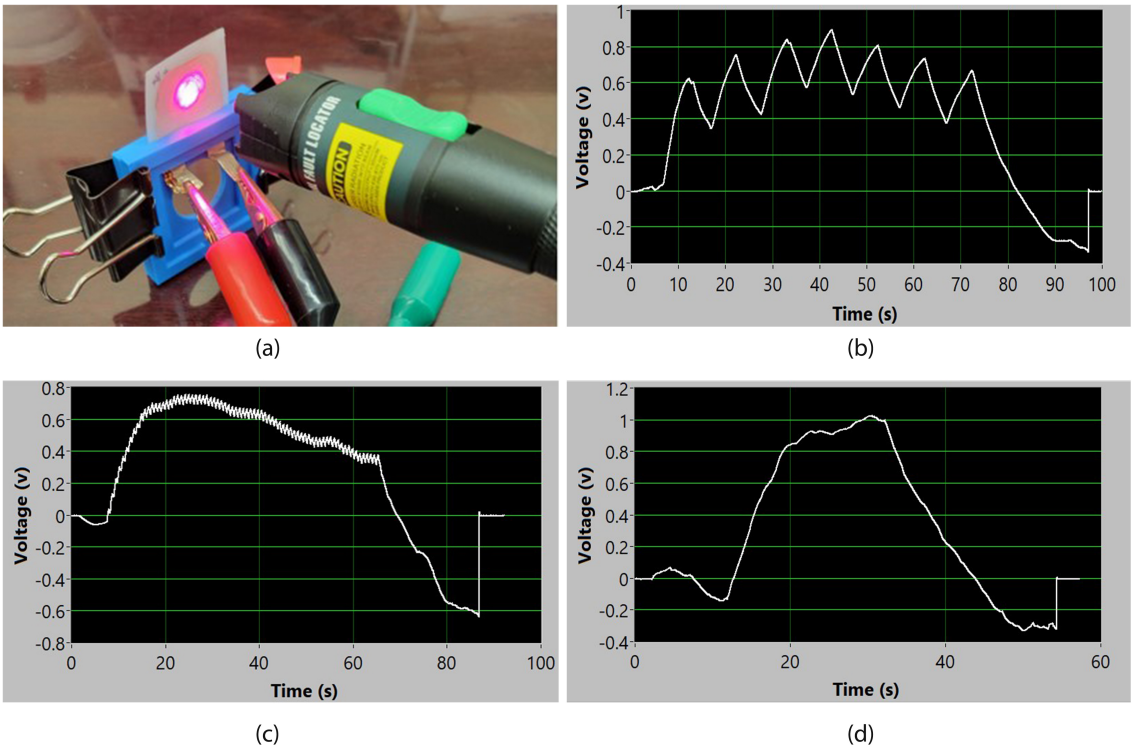

Figure 4.9: Pyroelectric response measurement setup (a). Laser blinking in 0.2 Hz (b) and in 1 Hz (c), and continuously shining on the surface (d).

Based on the observed piezoelectric and pyroelectric results, a set of experiments was designed to understand how corona poling parameters affect the samples' responses. A total of three poling parameters were selected for this purpose: the corona discharge voltage, poling time, and needle-sample distance. Table 4.2 lists the values for these parameters. It is also important to note here that temperature is another important parameter. It is well known that poling PVDF and its copolymers at higher temperatures ($\leq 80°C$) improves the polarization process due to higher mobility of the polymer chains. However, this parameter was considered for future research due

Table 4.2: Initial parameters selected for studying corona poling process.

Parameter	**Magnitude**	**Reference Figure**
Corona voltage	15, 19, 22 kV	4-11 (a)
Poling time	30, 60, 300 s	4-11 (b)
Needle to sample distance	20 and 40 mm	4-11 (c)

to the importance of investigating it as part of simultaneous printing and poling. As a precaution against possible damages to the printer caused by high electrical shocks from potential breakdowns, the tests were conducted on the same poling station that was previously used for poling samples.

A visual inspection was performed prior to poling of the samples to ensure that they are free of defects such as holes and gaps. The presence of defects in the sample increases the possibility of early breakdown and prevents the accumulation of charges since charges can escape to the grounded electrode. Despite this, electrical breakdown occurred multiple times, which may be caused by multiple factors including undetected sample defects or a high electric field intensity that the sample could not withstand. In this chapter, results are presented for samples with no breakdown during poling.

The effects of the selected parameters on the pyroelectric output can be clearly seen in Figure 4.10. Rather than generating complex 3D figures, only the effect of the parameter of interest is depicted in each graph, while the other two parameters kept constant at their maximums, except for the needle-sample distance, which was set at 20 mm when investigating another parameter.

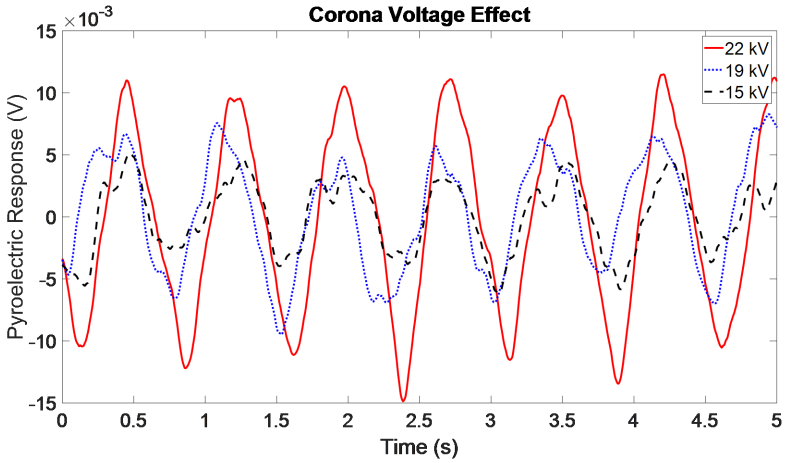

(a)

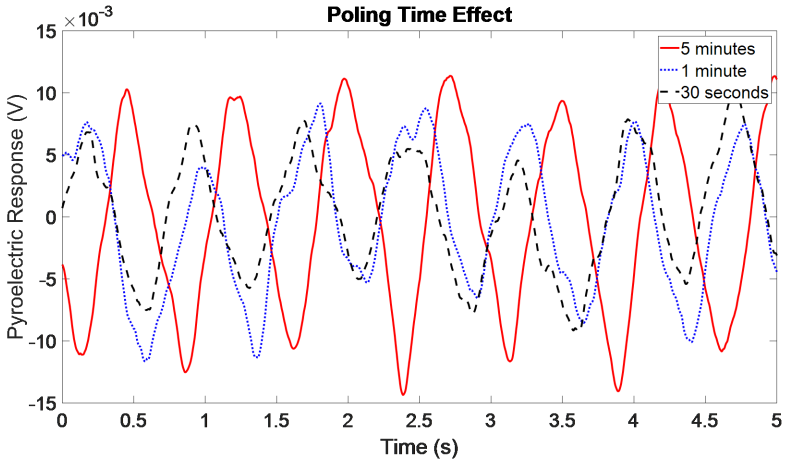

(b)

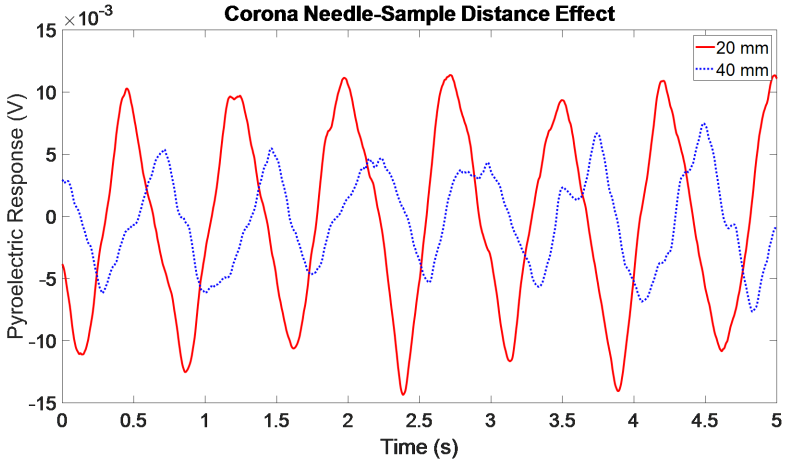

(c)

Figure 4.10: : The effect of corona voltage (a), poling time (b) and needle-sample distance (c) on pyroelectric response of PVDF-TrFE samples.

As expected, the general trend that can be seen in Figure 4.10 suggests reducing the distance, increasing the voltage, and poling time to increase the output response. However, the occurrence of electrical breakdown and other poling issues that will be discussed later limit the increasing or decreasing of these parameters. Furthermore, these settings are coupled, and therefore, changing one parameter affects the other parameter. For instance, decreasing the needle-sample distance limits the maximum corona voltage, or increasing the voltage could expedite the occurrence of electrical breakdown and hence reduce the poling time.

Based on these results, and to find any probable existing saturation poling time, samples were also poled for 10 minutes. Since poling the samples for more than 5 minutes at 22 kV and 40 mm did not result in any breakdown, the voltage for this distance was increased to 25 kV. However, at 20 mm and 22 kV, the breakdown was observed multiple times around 5 minutes. Therefore, for poling at 20 mm for 10 minutes, the voltage was lowered to 20 kV which resulted in stable poling with no breakdown. It can be seen from the results shown in Figure 4.11 that increasing the poling time for the samples from 1 to 5 minutes creates a stable response while increasing the poling time from 5 to 10 minutes has a small effect on the magnitude of the response. Furthermore, increasing the poling time for larger needle-sample distance has more noticeable effect on the response. This can be clearly seen in Figure 4.12.

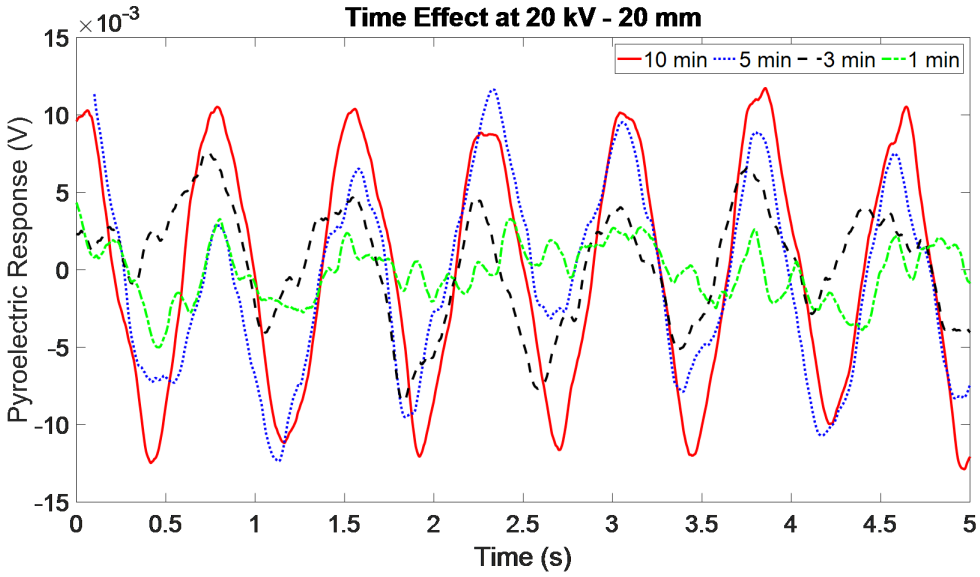

(a)

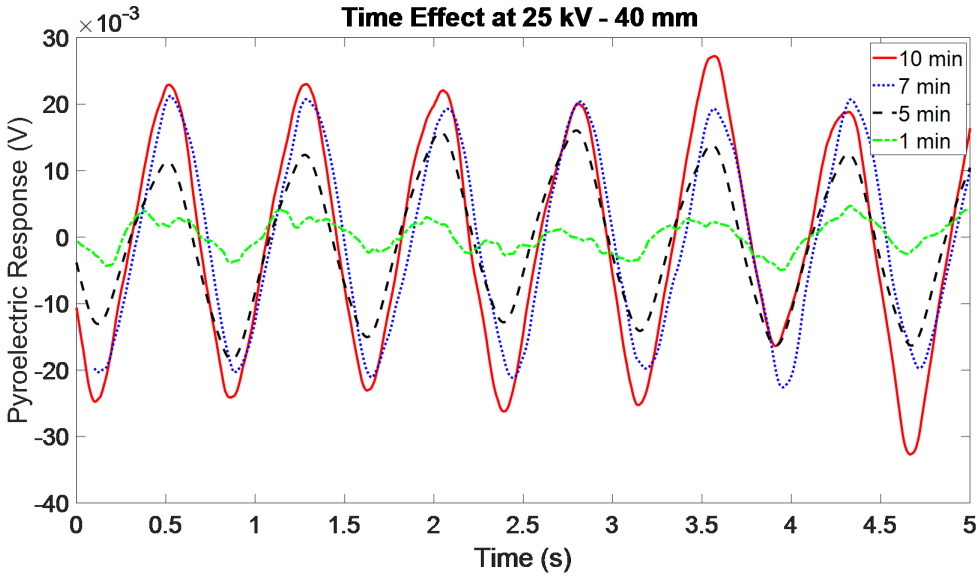

(b)

Figure 4.11: : The effect of extended poling time on the pyroelectric response while corona parameters were set to 20 kV at 20 mm (a) and 25 kV at 40 mm (b).

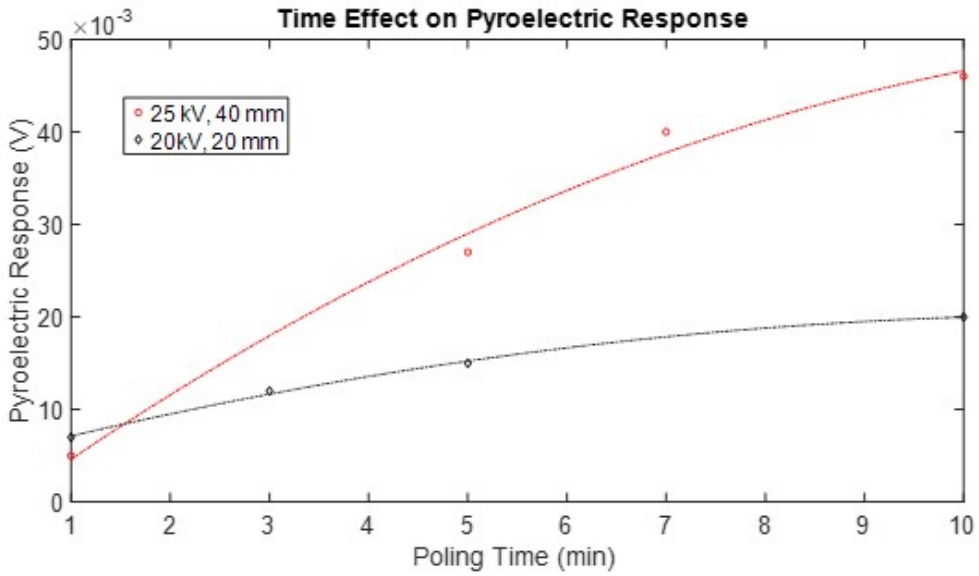

Figure 4.12: : Effects of poling time on pyroelectric response at 25 kV corona voltage and 40 mm needle-sample distance (red), and 20 kV corona voltage and 20 mm needle-sample distance (black).

To investigate the effect of poling time on the magnitude of polarization through the thickness of samples, the pyroelectric response of both the front and back surfaces of the sample was measured where "front surface" is the surface under the needle and "back surface" is the surface touching the grounded electrode. It can be inferred that the material closer to the top surface shows a higher degree of polarization. However, as poling time increases, this gradient in polarization magnitude through the thickness decreases.

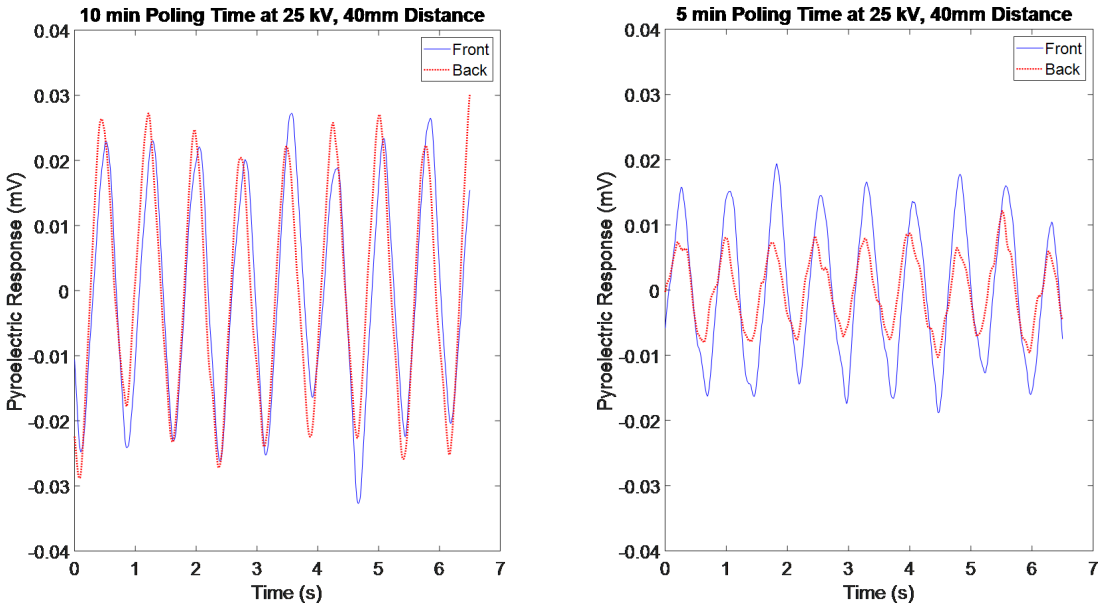

(a) (b)

Figure 4.13: Effects of sample orientation on the pyroelectric response for the sample poled under 25 kV at 40 mm needle-sample distance for 10 min (a) and 5 min (b).

The quality of the sample's print or its lack of holes and gaps, as highlighted multiple times in this document, hugely affects poling success. Observations showed that crack-containing samples with high corona voltages experience electrical breakdown after one minute. It is possible for the breakdown to occur continuously or intermittently, based on the magnitude of the corona voltage and the needle-sample distance. It is therefore necessary to pay special attention to sample preparation. Another problem encountered during the poling process was charge leakage to the ground electrode. This can be explained by the gap between the sample and the ground electrode around its edges. 3D printed samples possess inherent curvature due to residual thermal stress, so they cannot be coupled with a ground electrode perfectly without external assistance. As a result of this gap between the sample edge and the ground electrode, charge runaway occurs, which interrupts the top surface charge buildup. Therefore, it is impossible to create an electric field strong enough to pole

the samples thoroughly. Kapton tape or conventional electrical tape could be used to cover the edges of the sample to prevent this issue to some degree, but not entirely. Some of the encountered issues during corona poling are illustrated in Figure 4.14. The blurriness of some of these pictures is due to lack of light and focusing issues of the camera lens.

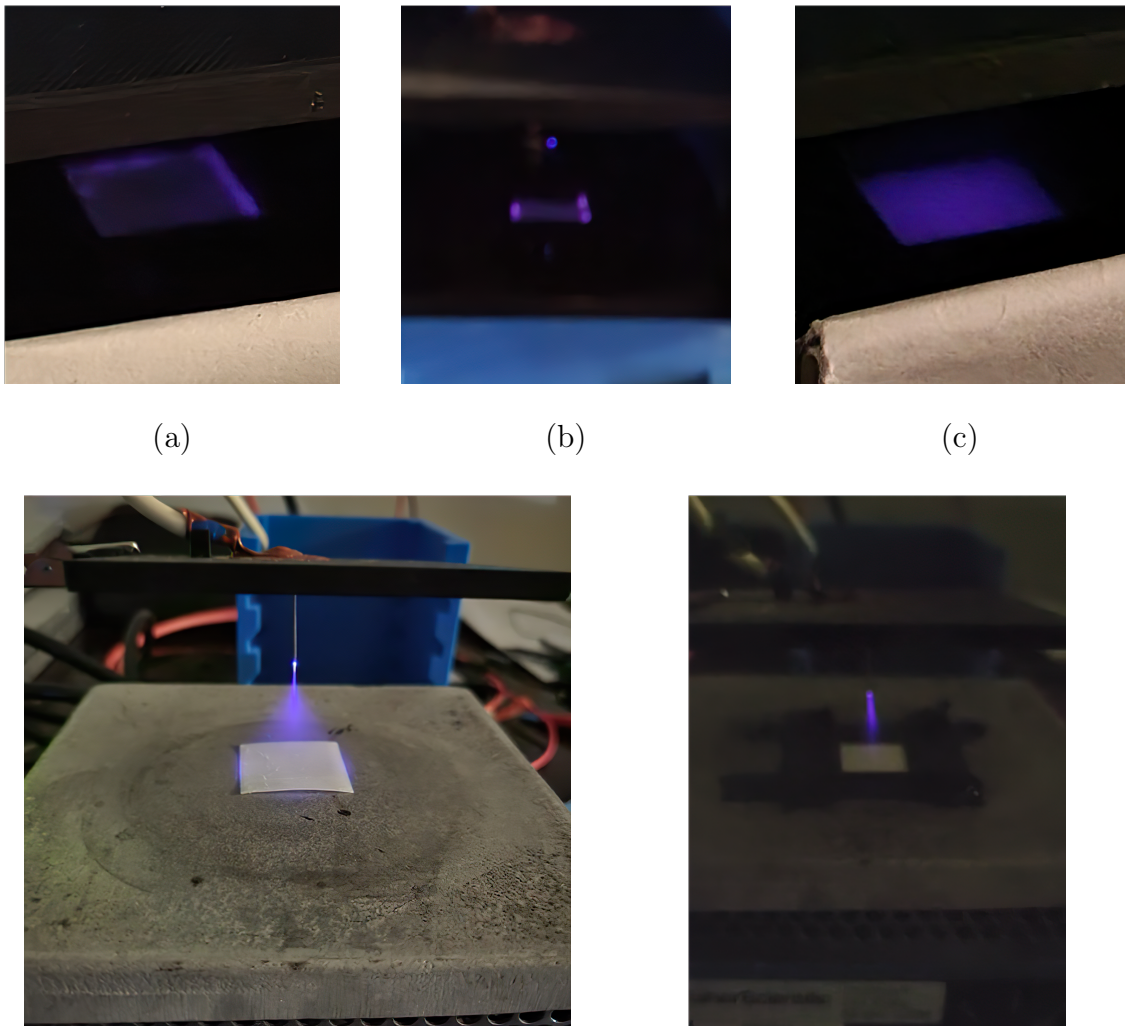

(a) (b) (c)

(d) (e)

Figure 4.14: Common issues observed during corona poling of the samples: (a) charge escaping around the edges, (b) localized charge escaping, (c) air gap under the sample which results in air ionization under the sample, (d) sample placed on the plate (ground electrode); no charge accumulated since all the charges freely escape to the ground, and (e) sample's edge covered with electrical tape. The corona ionization cone got narrower compared to (d).

CHAPTER 5: CONCLUSION AND FUTURE WORK

In response to thermophysical stress, certain materials generate an electric charge due to their piezoelectric properties. Piezoelectric polymers offer considerable promise for use in various fields due to their light weight, flexibility, and ease of processing. Common manufacturing methods are typically limited to simple geometry such as thin films. However, with recent rapid advancements in additive manufacturing technologies, this method has drawn a great deal of interest in creating more complex shapes for sensors. Fabricating 3D printed polymer-based sensors allows manufacturing of complex parts with high precision, reduced waste, and improved design flexibility. In theory, 3D printed piezoelectric sensors would be extremely promising. However, the scientific state of the art regarding the polymers, manufacturing process, and suitable conditions for manufacturing such sensors is uninvestigated.

This work started by adopting the fundamental concepts of Electric poling-assisted additive manufacturing (EPAM) method proposed by Lee and Tarbutton [3], in which the PVDF was 3D printed and poled with a customized Fused Deposition Modeling (FDM) method. This method was developed with the hypothesis that the mechanical stress applied to the molten PVDF due to the high pressure inside the nozzle during the extrusion process and the mechanical stretching happening in molten PVDF strung from the printer's bed to the nozzle, along with the simultaneous application of a high electric field, would result in the formation of the β-phase conformation with aligned dipoles. However, since the stretching (applied stress) and poling process during EPAM were conducted at temperatures greater than 200 °C, that is well above the restricted temperature of β-phase formation $\sim$ 100-150 °C [35, 70], the printed samples were still mainly in the non-polar α-phase. Furthermore, the applied electric

field during EPAM was limited to a small magnitude due to the electrical breakdown occurring between the nozzle and the printer bed. To overcome these shortcomings, in this research, PVDF was replaced with PVDF-TrFE, which always results in β-phase crystallization from the melt. Furthermore, the corona discharge method was employed as the poling process to achieve higher electric fields. To better investigate the effect of corona discharge performance on poling the samples, it was separated from the printing process to achieve high electrical fields while minimizing the chance of damaging the printer due to electrical breakdown.

Based on X-ray Diffraction (XRD) analysis of the additively manufactured samples using FDM printing, PVDF-TrFE resulted in nearly pure β-phase fabricated samples. The samples were poled with the corona discharge method both at room temperature and at a raised temperature (80 °C) using a hot plate. The samples that were poled without any occurrence of electrical breakdown were then tested to measure their piezoelectric response. For the free-end cantilever test with a 5 mm displacement, a single-layer PVDF-TrFE sample exhibited a piezoelectric response of 0.65 V. By printing double-layer samples that consist of a piezoactive layer (PVDF-TrFE) printed on a non-piezoactive layer (PVDF) as a substrate, larger stress was induced in the electroactive layer, resulting in a higher piezoelectric response. The flickering of a simple 20×30 mm sample (15×25 mm covered with silver paint as the electrode) resulted in an output voltage as high as 130 V peak-to-peak. Moreover, a piezoelectric response of 19 V was observed for a 2 mm cyclic displacement using a fatigue test machine (BOSE Electroforce 3200).

Furthermore, the successfully poled samples showed pyroelectric response, which was expected for PVDF-TrFE, since its pyroelectric property is well known. The preliminary pyroelectric response of the prepared samples was measured by shining a 30 mW laser at them. Since a higher degree of polarization in the material (or more aligned dipoles in the direction of the applied electric field) results in a higher

pyroelectric response, therefore, this property was used to investigate the effect of corona poling parameters on polarization degree. Samples with no visible defects such as holes and gaps which result in poling failure were used for this purpose. Corona voltage that is applied to the needle, poling duration, and needle-sample distance were selected as the parameters of interest. Despite the known importance of the poling temperature, this parameter was put aside for future work because it is worth investigating in the simultaneous printing and poling procedure. The trends found in the results indicate that increasing voltage and poling duration and decreasing needle-sample distance results in better polarization, only if these parameters are studied individually by keeping. However, it was clear that these parameters are coupled, and changing one parameter limits the others. A distinct example for this was observed for shorter needle-sample distance which limited the achievable maximum corona voltage and poling duration due to expediting the occurrence of electrical breakdown. It was also found that poling at a larger electrodes gap (40 mm) at higher voltage (25 kV) results in better polarization compared to closer electrodes distance (20 mm) and lower limited voltage (20 kV).

The obtained results in this research show that additive manufacturing of PVDF-TrFE alongside with corona poling method, can be a promising method with high repeatability and reproducibility for manufacturing piezo- and pyroelectric polymer-based sensors. However, to fully benefit from the potential of additive manufacturing in making these sensors, more research is required to be able to combine printing and poling processes in a single step process. The following are the proposed future research topics that need to be addressed.

1. Improving the quality of the printed parts to minimize the presence of defects is the first important topic that can be addressed. Samples with gaps, holes, voids, etc., cannot withstand high electric fields and therefore it is almost impossible to effectively pole them. For this purpose, more tests need to be done for

making high quality filament. The ideal filament should have a circular cross section with 1.75 mm diameter. Small deviation from this ideal diameter can be addressed during setting the print parameters, however, this only works if we have a "systematic error" in the diameter of the filament. This means that print settings can be adjusted for a filament with a different diameter from the ideal 1.75 mm, but this difference must be consistent for the whole length of the filament. With enough material in hand, this can be achieved by trial and error to find the best settings for filament extruder. The print quality also can also be optimized with the help of material characterization methods such as SEM and DCS, to better understand the effect of print parameters on the material structure of the samples and detect the microscopic defects.

2. The Corona poling process needs to be done under more controlled conditions so it can be later combined with the printing process. The main question in this regard would be how to confine the traveling of created ions and charges due to the corona wind effect. It might be useful to perform corona poling using 2 high voltage power supplies with the same polarity with one connected to the corona needle and the other one applying a biased voltage to a conductive ring around the sample that prevents the charges to migrate to the surrounding. However, implementing this technique in the 3D printer could be challenging. The effect of poling temperature is another important parameter that needs to be studied. The corona voltage could be decreased as we know poling can be more effective at elevated temperatures, and therefore it might be easier to control the charged particles. Higher temperatures can be achieved by the printer bed because it is set to +60 °C during the print for better layer adhesion.

3. One of the most attractive goals of using additive manufacturing in this field is to create multi-layer or stacked piezoelectric sensors without the need for post

processing steps. To achieve this, each printed layer must be poled before the electrode is applied to its top surface, and then repeat this procedure. The main concern in this procedure is that printing the new layer would increase the temperature of the previous layer to the level that destroys its polarization. In FDM method, layers are fused to the adjacent layers, meaning that they melt the previous layer at the contacting area, which in the case of a poled piezoelectric PVDF-TrFE layer results in losing the polarization. However, it might be possible to apply a layer of a heat resistant material that can adhere to the previously printed sample to prevent excessive heat transfer from printing the next layer.

REFERENCES

[1] H. Kawai, "The piezoelectricity of poly(vinylidene fluoride)," *Japanese Journal of Applied Physics*, vol. 8, pp. 975–976, 1969.

[2] H. Li, R. Wang, S.-T. Han, and Y. Zhou, "Ferroelectric polymers for non-volatile memory devices: a review," *Polymer International*, vol. 69, no. 6, pp. 533–544, 2020.

[3] L. ChaBum and A. T. Joshua, "Electric poling-assisted additive manufacturing process for pvdf polymer-based piezoelectric device applications," *Smart Materials and Structures*, vol. 23, no. 9, p. 095044, 2014.

[4] H. Jaffe, *Piezoelectric ceramics*, vol. 41 of *Journal of the American Ceramic Society*. 1958.

[5] I. Katsouras, K. Asadi, M. Li, T. B. van Driel, K. S. Kjær, D. Zhao, T. Lenz, Y. Gu, P. W. M. Blom, D. Damjanovic, M. M. Nielsen, and D. M. de Leeuw, "The negative piezoelectric effect of the ferroelectric polymer poly(vinylidene fluoride)," *Nature Materials*, vol. 15, no. 1, pp. 78–84, 2016.

[6] P. Muralt, *Pyroelectricity*, pp. 441–448. Oxford: Elsevier, 2005.

[7] S. Bauer and S. B. Lang, "Pyroelectric polymer electrets," *IEEE Transactions on Dielectrics and Electrical Insulation*, vol. 3, no. 5, pp. 647–676, 1996.

[8] J. A. Gallego-Juarez, "Piezoelectric ceramics and ultrasonic transducers," *Journal of Physics E: Scientific Instruments*, vol. 22, no. 10, p. 804, 1989.

[9] J. F. Tressler, S. Alkoy, and R. E. Newnham, "Piezoelectric sensors and sensor materials," *Journal of Electroceramics*, vol. 2, no. 4, pp. 257–272, 1998.

[10] R. C. Turner, P. A. Fuierer, R. E. Newnham, and T. R. Shrout, "Materials for high temperature acoustic and vibration sensors: A review," *Applied Acoustics*, vol. 41, no. 4, pp. 299–324, 1994.

[11] D. J. Inman, *Energy Harvesting Technologies*. Boston, MA: Springer US, 2009.

[12] A. Manbachi and R. S. C. Cobbold, "Development and application of piezoelectric materials for ultrasound generation and detection," *Ultrasound*, vol. 19, no. 4, pp. 187–196, 2011.

[13] N. Jalili, *Piezoelectric-based vibration control: from macro to micro/nano scale systems*. Springer Science Business Media, 2009.

[14] E. Hollenstein, D. Damjanovic, and N. Setter, "Temperature stability of the piezoelectric properties of li-modified knn ceramics," *Journal of the European Ceramic Society*, vol. 27, no. 13, pp. 4093–4097, 2007.

[15] *Ferroelectric polymers: chemistry, physics, and applications*. Plastics engineering ; 28, New York: M. Dekker, Inc., 1995.

[16] F. V. Cardoso, M. D. Correia, C. Ribeiro, M. M. Fernandes, and S. Lanceros-Méndez, "Fluorinated polymers as smart materials for advanced biomedical applications," *Polymers*, vol. 10, no. 2, 2018.

[17] O. Sharon Rosyln, W. Ting Chong, T. Chin Yaw, Y. Kui, and T. Francis Eng-Hock, "Fabrication of piezoelectric polymer multilayers on flexible substrates for energyÂ harvesting," *Smart Materials and Structures*, vol. 23, no. 1, p. 015013, 2014.

[18] Y.-H. Shin, I. Jung, M.-S. Noh, J. H. Kim, J.-Y. Choi, S. Kim, and C.-Y. Kang, "Piezoelectric polymer-based roadway energy harvesting via displacement amplification module," *Applied Energy*, vol. 216, pp. 741–750, 2018.

[19] R. Schellin, G. Hess, R. Kressman, and P. Wassmuth, "Corona-poled piezoelectric polymer layers of p(vdf/trfe) for micromachined silicon microphones," *Journal of Micromechanics and Microengineering*, vol. 5, no. 2, p. 106, 1995.

[20] P.-H. Ducrot, I. Dufour, and C. Ayela, "Optimization of pvdf-trfe processing conditions for the fabrication of organic mems resonators," *Scientific Reports*, vol. 6, p. 19426, 2016.

[21] P. Martins, A. C. Lopes, and S. Lanceros-Mendez, "Electroactive phases of poly(vinylidene fluoride): Determination, processing and applications," *Progress in Polymer Science*, vol. 39, no. 4, pp. 683–706, 2014.

[22] J. Lovinger Andrew, "Crystallization and morphology of melt-solidified poly(vinylidene fluoride)," *Journal of Polymer Science: Polymer Physics Edition*, vol. 18, no. 4, pp. 793–809, 1980.

[23] W. M. Prest and D. J. Luca, "The morphology and thermal response of high-temperature-crystallized poly(vinylidene fluoride)," *Journal of Applied Physics*, vol. 46, no. 10, pp. 4136–4143, 1975.

[24] H. Pan, B. Na, R. Lv, C. Li, J. Zhu, and Z. Yu, "Polar phase formation in poly(vinylidene fluoride) induced by melt annealing," *Journal of Polymer Science Part B: Polymer Physics*, vol. 50, no. 20, pp. 1433–1437, 2012.

[25] A. J. Lovinger, *Poly(Vinylidene Fluoride)*, pp. 195–273. Dordrecht: Springer Netherlands, 1982.

[26] J. Wu, X. Sun, S. Zhu, J. Bai, X. Zhu, J. Dai, L. Yin, W. Song, and Y. Sun, "Magnetic field induced formation of ferroelectric β phase of poly (vinylidene fluoride)," *Applied Physics A*, vol. 126, no. 8, p. 624, 2020.

[27] A. J. Lovinger, "Unit cell of the γ phase of poly(vinylidene fluoride)," *Macromolecules*, vol. 14, no. 2, pp. 322–325, 1981.

[28] M. Li, H. J. Wondergem, M.-J. Spijkman, K. Asadi, I. Katsouras, P. W. M. Blom, and D. M. de Leeuw, "Revisiting the δ-phase of poly(vinylidene fluoride) for solution-processed ferroelectric thin films," *Nature Materials*, vol. 12, no. 5, pp. 433–438, 2013.

[29] A. J. Lovinger, "Annealing of poly(vinylidene fluoride) and formation of a fifth phase," *Macromolecules*, vol. 15, no. 1, pp. 40–44, 1982.

[30] P. D. Southgate, "Room-temperature poling and morphology changes in pyroelectric polyvinylidene fluoride," *Applied Physics Letters*, vol. 28, no. 5, pp. 250–252, 1976.

[31] A. Salimi and A. A. Yousefi, "Analysis method: Ftir studies of β-phase crystal formation in stretched pvdf films," *Polymer Testing*, vol. 22, no. 6, pp. 699–704, 2003.

[32] K. Matsushige, K. Nagata, S. Imada, and T. Takemura, "The ii-i crystal transformation of poly(vinylidene fluoride) under tensile and compressional stresses," *Polymer*, vol. 21, no. 12, pp. 1391–1397, 1980.

[33] C. Lee and J. A. Tarbutton, "Polyvinylidene fluoride (pvdf) direct printing for sensors and actuators," *The International Journal of Advanced Manufacturing Technology*, vol. 104, no. 5, pp. 3155–3162, 2019.

[34] D. Y. Y. Chen, "beta-phase formation of poly(vinylidene fluoride) from the melt induced by quenching," *Materials science letters*, vol. 6, pp. 599–603, 1987.

[35] H. W. Siesler, "Rheo-optical fourier-transform infrared spectroscopy of polymers. 9. stretching-induced ii(α))-i(β) crystal phase transformation in poly(vinylidene fluoride)," *Journal of Polymer Science: Polymer Physics Edition*, vol. 23, no. 12, pp. 2413–2422, 1985.

[36] V. Sencadas, R. Gregorio, and S. Lanceros-Méndez, "α to β phase transformation and microestructural changes of pvdf films induced by uniaxial stretch," *Journal of Macromolecular Science, Part B*, vol. 48, no. 3, pp. 514–525, 2009.

[37] G. T. Davis, J. E. McKinney, M. G. Broadhurst, and S. Roth, "Electric-field-induced phase changes in poly(vinylidene fluoride)," *Journal of Applied Physics*, vol. 49, 1978.

[38] G. W. Day, C. A. Hamilton, R. L. Peterson, R. J. Phelan, and L. O. Mullen, "Effects of poling conditions on responsivity and uniformity of polarization of pvf2 pyroelectric detectors," *Applied Physics Letters*, vol. 24, no. 10, pp. 456–458, 1974.

[39] A. Roggero, E. Dantras, and C. Lacabanne, "Poling influence on the mechanical properties and molecular mobility of highly piezoelectric p(vdf-trfe) copolymer," *Journal of Polymer Science Part B: Polymer Physics*, vol. 55, no. 18, pp. 1414–1422, 2017.

[40] D. K. Das Gupta and K. Doughty, "Changes in x-ray diffraction patterns of polyvinylidene fluoride due to corona charging," *Applied Physics Letters*, vol. 31, no. 9, pp. 585–587, 1977.

[41] J. M. Kenney and S. C. Roth, "Room temperature poling of poly(vinylidene fluoride) with deposited metal electrodes," *Journal of Research of the National Bureau of Standards*, vol. 84, 1979.

[42] J. B. Lando and W. W. Doll, "The polymorphism of poly(vinylidene fluoride). i. the effect of head-to-head structure," *Journal of Macromolecular Science, Part B*, vol. 2, no. 2, pp. 205–218, 1968.

[43] B. L. Farmer, A. J. Hopfinger, and J. B. Lando, "Polymorphism of poly(vinylidene fluoride): potential energy calculations of the effects of head-to-head units on the chain conformation and packing of poly(vinylidene fluoride)," *Journal of Applied Physics*, vol. 43, no. 11, pp. 4293–4303, 1972.

[44] K. Koga and H. Ohigashi, "Piezoelectricity and related properties of vinylidene fluoride and trifluoroethylene copolymers," *Journal of Applied Physics*, vol. 59, no. 6, pp. 2142–2150, 1986.

[45] S. Chen, K. Yao, F. Tay, and L. Li Shan Chew, *Comparative Investigation of the Structure and Properties of Ferroelectric Poly(vinylidene fluoride) and Poly(vinylidene fluoride-trifluoroethylene) Thin Films Crystallized on Substrates*, vol. 116. 2010.

[46] A. Salimi and A. A. Yousefi, "Conformational changes and phase transformation mechanisms in pvdf solution-cast films," *Journal of Polymer Science Part B: Polymer Physics*, vol. 42, no. 18, pp. 3487–3495, 2004.

[47] E. Fontananova, J. C. Jansen, A. Cristiano, E. Curcio, and E. Drioli, "Effect of additives in the casting solution on the formation of pvdf membranes," *Desalination*, vol. 192, no. 1, pp. 190–197, 2006.

[48] Z. Yin, B. Tian, Q. Zhu, and C. Duan, "Characterization and application of pvdf and its copolymer films prepared by spin-coating and langmuir-blodgett method," *Polymers*, vol. 11, no. 12, p. 2033, 2019.

[49] S. Ramasundaram, S. Yoon, K. J. Kim, and J. S. Lee, "Direct preparation of nanoscale thin films of poly (vinylidene fluoride) containing β-crystalline phase by heat-controlled spin coating," *Macromolecular Chemistry and Physics*, vol. 209, no. 24, pp. 2516–2526, 2008.

[50] G. Kalimuldina, N. Turdakyn, I. Abay, A. Medeubayev, A. Nurpeissova, D. Adair, and Z. Bakenov, "A review of piezoelectric pvdf film by electrospinning and its applications," *Sensors*, vol. 20, no. 18, p. 5214, 2020.

[51] E. S. Cozza, O. Monticelli, E. Marsano, and P. Cebe, "On the electrospinning of pvdf: Influence of the experimental conditions on the nanofiber properties," *Polymer International*, vol. 62, no. 1, pp. 41–48, 2013.

[52] O. Pabst, J. Perelaer, E. Beckert, U. S. Schubert, R. Eberhardt, and A. Tunnermann, "All inkjet-printed piezoelectric polymer actuators: Characterization and applications for micropumps in lab-on-a-chip systems," *Organic Electronics*, vol. 14, no. 12, pp. 3423–3429, 2013.

[53] D. Thuau, K. Kallitsis, F. D. Dos Santos, and G. Hadziioannou, "All inkjet-printed piezoelectric electronic devices: energy generators, sensors and actuators," *Journal of Materials Chemistry C*, vol. 5, no. 38, pp. 9963–9966, 2017.

[54] R. L. Truby and J. A. Lewis, "Printing soft matter in three dimensions," *Nature*, vol. 540, no. 7633, pp. 371–378, 2016.

[55] C. Chen, X. Wang, Y. Wang, D. Yang, F. Yao, W. Zhang, B. Wang, G. A. Sewvandi, D. Yang, and D. Hu, "Additive manufacturing of piezoelectric materials," *Advanced Functional Materials*, vol. 30, no. 52, p. 2005141, 2020.

[56] H. Kim, L. C. D. Manriquez, M. T. Islam, L. A. Chavez, J. E. Regis, M. A. Ahsan, J. C. Noveron, T.-L. B. Tseng, and Y. Lin, "3d printing of polyvinylidene fluoride/photopolymer resin blends for piezoelectric pressure sensing application using the stereolithography technique," *MRS Communications*, vol. 9, no. 3, pp. 1115–1123, 2019.

[57] A. Wang, C. Chen, L. Liao, J. Qian, F.-G. Yuan, and N. Zhang, "Enhanced β-phase in direct ink writing pvdf thin films by intercalation of graphene," *Journal of Inorganic and Organometallic Polymers and Materials*, vol. 30, no. 5, pp. 1497–1502, 2020.

[58] R. S. Pinto, J. P. Serra, J. C. Barbosa, R. Goncalves, M. M. Silva, S. Lanceros-Mendez, and C. M. Costa, "Direct-ink-writing of electroactive polymers for sensing and energy storage applications," *Macromolecular Materials and Engineering*, vol. 306, no. 11, p. 2100372, 2021.

[59] D. A. Porter, T. V. T. Hoang, and T. A. Berfield, "Effects of in-situ poling and process parameters on fused filament fabrication printed pvdf sheet mechanical and electrical properties," *Additive Manufacturing*, vol. 13, pp. 81–92, 2017.

[60] K. Hoejin, T. Fernando, W. Yanyu, V. Dino, L. Yirong, and T. Tzu-Liang, "Integrated 3d printing and corona poling process of pvdf piezoelectric films for pressure sensor application," *Smart Materials and Structures*, vol. 26, no. 8, p. 085027, 2017. (Bill).

[61] X. Yuan, X. Gao, J. Yang, X. Shen, Z. Li, S. You, Z. Wang, and S. Dong, "The large piezoelectricity and high power density of a 3d-printed multilayer copolymer in a rugby ball-structured mechanical energy harvester," *Energy Environmental Science*, vol. 13, no. 1, pp. 152–161, 2020.

[62] J. Tarbutton, T. Leb, G. Helfrichb, and M. Kirkpatrickb, "Phase transformation and shock sensor response of additively manufactured piezoelectric pvdf," *Procedia Manufacturing*, vol. 10, pp. 982–989, 2017.

[63] X. Liu, Y. Shang, J. Zhang, and C. Zhang, "Ionic liquid-assisted 3d printing of self-polarized β-pvdf for flexible piezoelectric energy harvesting," *ACS Applied Materials Interfaces*, vol. 13, no. 12, pp. 14334–14341, 2021. doi: 10.1021/acsami.1c03226.

[64] H. Pei, Y. Xie, Y. Xiong, Q. Lv, and Y. Chen, "A novel polarization-free 3d printing strategy for fabrication of poly (vinylidene fluoride) based nanocomposite piezoelectric energy harvester," *Composites Part B: Engineering*, vol. 225, p. 109312, 2021.

[65] C. Chen, F. Cai, Y. Zhu, L. Liao, J. Qian, F.-G. Yuan, and N. Zhang, "3d printing of electroactive pvdf thin films with high β-phase content," *Smart Materials and Structures*, vol. 28, no. 6, p. 065017, 2019.

[66] W.-S. Jung, M. Lee, S.-H. Baek, I. K. Jung, S.-J. Yoon, and C.-Y. Kang, "Structural approaches for enhancing output power of piezoelectric polyvinylidene fluoride generator," *Nano Energy*, vol. 22, pp. 514–523, 2016.

[67] W.-S. Jung, M.-G. Kang, H. G. Moon, S.-H. Baek, S.-J. Yoon, Z.-L. Wang, S.-W. Kim, and C.-Y. Kang, "High output piezo/triboelectric hybrid generator," *Scientific Reports*, vol. 5, p. 9309, 2015.

[68] J. A. Giacometti and O. N. Oliveira, "Corona charging of polymers," *IEEE Transactions on Electrical Insulation*, vol. 27, no. 5, pp. 924–943, 1992.

[69] M. Goldman, A. Goldman, and R. S. Sigmond, "The corona discharge, its properties and specific uses," *Pure and Applied Chemistry*, vol. 57, pp. 1353 – 1362, 1985.

[70] W. T. Mead, A. E. Zachariades, T. Shimada, and R. S. Porter, "Solid state extrusion of poly(vinylidene fluoride). 1. ram and hydrostatic extrusion," *Macromolecules*, vol. 12, no. 3, pp. 473–478, 1979.